공학석사학위논문

열 효과 및 초음속 흐름을 고려한 압전 적층복합재료에 미소기계적 물성 응용

Analysis of Effective Properties in Smart Multilayered Plates in Thermal Environment and Supersonic Flow

2018 년 8 월

서울대학교 대학원

기계항공공학부

임 정 수

열 효과 및 초음속 흐름을 고려한 압전 적층복합재료에 미소기계적 물성 응용

Analysis of Effective Properties in Smart Multilayered Plates in Thermal Environment and Supersonic Flow

지도교수 김 지 환

이 논문을 공학석사 학위논문으로 제출함

2018 년 6 월

서울대학교 대학원

기계항공공학부

임 정 수

임정수의 공학석사 학위논문을 인준함

2018 년 6 월

위 원 장 _____

부위원장 _____

위 원 _____

Abstract

Currently, the analysis of composite laminates is limited by the moduli of the materials provided by experiments. However, this impedes research as the determining of the moduli for even a few composite materials with varying fiber volume fractions is economically unrealistic. As solution, the application of a micromechanical model based on the Representative Volume Element (RVE) is suggested. The model allows for the generalization of composite material by calculating its effective moduli. This study uses the finite element method (FEM) based on the First-order Shear Deformation Theory of Plates (FSDTP) that is applied to a generalized piezoelectric composite laminate plate. To verify the accuracy of the micromechanical moduli, the structure is investigated under distributed loads, voltages, temperatures and dynamic pressures in linear and nonlinear methods. The nonlinear analysis is performed using the Newton-Raphson Iterative method. In all cases, the micromechanical model was in good agreement with the experimental model. Also, an improved shear correction factor (SCF) was implemented to allow for further generalizations in the context of thick plate structures. Additionally, the application of Macro-Fiber Composites (MFC) piezoelectric layers instead of isotropic piezoelectric layers is investigated. As MFC piezo layers have a directional application of force, there was a greater shape control effect when compared to the conventional isotropic piezoelectric layers. Furthermore, as the MFC layers can be treated as unidirectional composite materials, their effective properties can also be determined with the micromechanical model.

Keywords: Micromechanical Model, Thermal Environment, Dynamic Pressure, Shear Correction Factor, Piezoelectric Materials, Nonlinear Analyses, Composite Laminate Plates

Student Number: 2016-26463

Contents

List of Tables and Figures

Tables

Figures

List of Nomenclature

Variables

$\mathbf{A}$	Extensional stiffness matrix
$\boldsymbol{A_d}$	Aerodynamic damping matrix
$\boldsymbol{A_f}$	Aerodynamic influence matrix
a	Length of the plate
$\mathbf{B}$	Bending-extension coupling stiffness matrix
b	Width of the plate
$\mathbf{D}$	Bending-twist coupling stiffness matrix
D_m	Bending rigidity
$\boldsymbol{d}$	Displacement
$[d]$	Piezoelectric strain constant matrix
E	Young's modulus
$\mathbf{e}$	In-plane strain vector
$\bar{e}$	Piezoelectric constant matrix
$\boldsymbol{F}$	Applied load vector
$\boldsymbol{F_{\Delta T}}$	Thermal load vector
$\boldsymbol{F_{pie}}$	Piezoelectric load vector
$\boldsymbol{f}$	External force vector
G	Shear modulus
G_d	Feedback control gain
g_a	Non-dimensional aerodynamic damping parameter
h	Thickness of the plate
$\boldsymbol{K}$	Linear elastic stiffness matrix
K	Shear correction factor
$\boldsymbol{K_{\Delta T}}$	Thermal stiffness matrix
$\boldsymbol{KN}_1$	First-order nonlinear stiffness matrix
$\boldsymbol{KN}_2$	Second-order nonlinear stiffness matrix
$\boldsymbol{M}$	Mass matrix
M_∞	Mach number
$\boldsymbol{M_b}$	In-plane moment resultant
$\boldsymbol{M_{\Delta T}}$	Thermal in-plane moment resultant
$\boldsymbol{N_b}$	In-plane force resultant
$\boldsymbol{N_{\Delta T}}$	Thermal in-plane force resultant
p_a	Aerodynamic pressure

$\overline{Q}$	Plane-stress reduced elastic constants
$q(t)$	Total charge
$\mathbf{S}$	Shear stiffness matrix
u	In-plane displacement in the x direction
u_0	Mid-plane displacement in the x direction
V	Volume fiber fraction
V_∞	Air flow speed
v	In-plane displacement in the y direction
v_0	Mid-plane displacement in the y direction
$\delta \boldsymbol{W}_{\text{int}}$	Internal virtual work
$\delta \boldsymbol{W}_{\text{ext}}$	External virtual work
w	In-plane displacement in the z direction
w_0	Mid-plane displacement in the z direction
Ξ	Permittivity coefficients
α	Coefficient of thermal expansion
β	Aerodynamic pressure parameter
ε	In-plane strain
ϕ_x	Rotation of the normal in the xz plane
ϕ_y	Rotation of the normal in the yz plane
$\boldsymbol{\gamma}$	Transverse shear strain vector
γ	Transverse shear strain
κ	Curvature strain
λ	Non-dimensional aerodynamic pressure
μ	Air-mass ratio
ρ_a	Air density
σ	In-plane stress
υ	Poisson's ratio
ω_0	Convenient reference frequency

Subscripts

f	Fiber
m	Matrix
c	Composite
e	Element
s	Static state
d	Dynamic state

1. Introduction

Composite laminate structures are of great importance in many fields of industry for its high strength to weight ratio. In particular, there has been extensive efforts in the fields of aerospace for lighter and stronger materials. This is due to the fact that many aerospace apparatuses and vehicles hinge upon being lightweight enough to achieve flight while still maintaining enough structural integrity to be operated safely. This is especially true for rockets and is well illustrated in the tyranny of the rocket equation. Without an adequately strong and simultaneously light material, a rocket will require more fuel to operate, which in turn increases the material needed to store enough fuel. This cycle is vicious and is often referred to as the tyranny of the rocket equation. Composite laminates fulfill that need in a simple yet efficient manner. In addition to composite laminates, piezoelectric materials are of great interest. With its ability to convert mechanical energy into electrical energy and vice versa, it has been given the name of "smart" material. Smart materials have proven to be flexible in application and have been incorporated in many structural models. Thus, it was inevitable that the two materials were combined into one.

As such, there have been numerous studies on the topic of piezoelectric composite laminates. Crawley and de Luis [1] have conducted an analysis of one-dimensional beams that have surface bonded and embedded piezo-actuators. This research was then expanded by Im and Atluri [2] through the inclusion of the shear forces exerted by the piezo-actuators. An analytical model was used by Lee [3] for sensors and actuators of a piezoelectric structure. They were applied for vibration control in rectangular laminate plates. Ha et al. [4] also studied the linear static and dynamic response in rectangular laminated composite plates with piezoelectric components. The active shape control capabilities of the piezoelectric composite laminate plate were shown by Lam

et al. [5], who used the Newmark-β method to show the transient response of the model. The structural model was then expanded to include the FSDTP by Detwiler et al. [6] and Huang and Wu [7]. The Navier solutions and the theoretical formulations of the piezoelectric composite laminate plate was provided by Reddy [8]. Batra et al. [9] then analyzed rectangular plates integrated with smart actuators with a simply-supported boundary condition. The geometrically nonlinear transient vibration analysis of the structure with actuators and sensors was performed by Moita [10] and Gao and Shen [11]. Fernandes and Pouget [12] provided a two-dimensional approach to the modeling of piezoelectric plates. They continued their research by including the piezo electric bimorph [13] and the laminated composites with piezoelectric elements [14]. The effects of active damping with piezoelectric patches were further studied by Saviz [15] using nonlinear vibrational analysis with composite plates. Then, the piezoelectric model was applied as a smart fin and was studied numerically and experimentally by Park et al. [16]. Additionally, thermal environments were also added the structural model. Lee and Saravanos [17] studied the thermal response of symmetric and antisymmetric composite plates with piezoelectric actuators. Additionally, Heidary and Eslami [18] performed dynamic analysis of piezothermoelastic composite plates using finite element methods based on the FSDTP. Sladek et al. [19] analyzed the crack problems for piezoelectric solid under a thermal load.

It can be observed that there is an extensive catalog of research that was invested into the smart multilayered composite structure. However, one thing that is consistent throughout is the dependency on experimentally determined moduli. As the topic of smart composite laminates continues to grow in scope and size, analysis is dependent on experiments to calculated the thermo-mechanical moduli of a composite material. This is a limitation on the composite materials that are available for analysis. Furthermore, the materials used in research cannot be generalized in

terms of the constituent materials or the fiber volume fraction. To avoid this limitation, the current work uses a micromechanical model based on the RVE method to calculate the thermo-mechanical moduli of a generalized composite material. The model is based on the FSDTP and has two smart layers surrounding the composite core. The element used in the finite element analysis is a nine-node element and has mechanical, thermal, and electrical forces applied to it. The effective moduli calculated from the model is verified through comparison of deflection calculated with moduli from other literatures. The deflection is conducted under various mechanical and electrical loads. Furthermore, a new SCF is introduced to the model, thus allowing for more accurate representations at varying thickness ratios. Additionally, the effects of MFC layers instead of isotropic piezoceramic layers are also investigated through shape control comparisons.

2. Formulation

The generalized structure in this work is a piezoelectric laminate composite structure. The composite laminate core of the plate is arranged in symmetric alternating ply-angles of $[\theta/\text{-}\theta]_s$ and is surrounded top and bottom by an isotropic piezoelectric layer. As shown in Fig. 1, the plate has the dimensions of length *a*, width *b*, and thickness *h*.

2.1 Micromechanical Model

Previously, composite material analysis was greatly dependent on experimental determined mechanical properties. However, that process is not economically viable for all variations of composite materials with varying volume fiber fractions. Thus, this work offers the application of a micromechanical model based on the RVE method to provide accurate estimations of mechanical moduli [20]. The total stress on the face of the material can be separated into a sum of stresses on the face of the fiber and the matrix. As such, the total stress can be expressed as a function of the volume fraction for the fiber and the matrix. Then, by utilizing the Rule of Mixtures (ROM), the longitudinal Young's modulus, *E*, for the composite can be represented as:

$$E_{1c} = E_{1f} v_f + E_m v_m \tag{1}$$

where the subscripts *c*, *f*, and *m* stand for the composite, fiber, and matrix, respectively. Additionally, *v* represents the volume faction of the composite. The same procedure can be repeated for the effective Poisson's ratio, υ. The major Poisson's ratio, υ_{12}, of the composite can

also be calculated using the major Poisson's ratio for the fiber, υ_{12f}, and matrix, υ_{12m} as in the similar equation in Ref. [10]:

$$\upsilon_{12} = \upsilon_{12f} v_f + \upsilon_{12m} v_m \tag{2}$$

Furthermore, the coefficients of thermal expansion, α_1 and α_2 must also be determined by ROM as in Ref. [21, 22]:

$$\alpha_{1c} = \frac{\alpha_{1f} E_{1f} v_f + \alpha_m E_m v_m}{E_{1f} v_f + E_m v_m} \tag{3}$$

where α_{1f} and α_m are the coefficient of longitudinal thermal expansion of the fiber and matrix, respectively. On the other hand, a different formula is used to calculate the coefficient of transverse thermal expansion, α_2, as in Ref. [22]:

$$\alpha_{2c} = (1+\upsilon_m)\alpha_m v_m + (1+\upsilon_{12f})\alpha_{2f} v_f - \alpha_1 \upsilon_{12} \tag{4}$$

where the α_{2f} is the coefficient of transverse thermal expansion of the fiber.

However, for the transverse Young's modulus, E_2 and the shear moduli, G_{12} and G_{23}, a different equation must be considered. This is due to the fact that these moduli are more sensitive to fiber geometry. Thus, a refined equation can be written as in Ref. [20]:

$$\begin{aligned}
E_{2c} &= E_m \left[\left(1-\sqrt{v_f}\right) + \frac{\sqrt{v_f}}{1-\sqrt{v_f}\left(1-E_m/E_{f2}\right)} \right] \\
G_{12c} &= G_m \left[\left(1-\sqrt{v_f}\right) + \frac{\sqrt{v_f}}{1-\sqrt{v_f}\left(1-G_m/G_{f12}\right)} \right] \\
G_{23c} &= G_m \left[\left(1-\sqrt{v_f}\right) + \frac{\sqrt{v_f}}{1-\sqrt{v_f}\left(1-G_m/G_{f23}\right)} \right]
\end{aligned} \tag{5}$$

The circular fiber area is first represented as a square that have side lengths that are a function of the diameter of the circle. Then, the shape is divided into the two regions, A and B. The overall modulus of section B can be calculated using the previous ROM. Then, the modulus of the entire element can then be derived by iterating the ROM once more. Through these methods, the effective mechanical moduli of the composite material can be derived using only the properties of the constituent materials and the volume fiber fraction. Additionally, it is worth noting that, as the piezoelectric layers are isotropic and do not contain fibers, this micromechanical model does not apply.

2.2 Constitutive Equations

The structural model that is used in this study is based on the FSDTP. As such, the variables *u*, *v*, and *w* denote displacements in the *x*, *y*, and *z* directions and the variables ϕ_x and ϕ_y represent the rotations about the *xz* and the *yz* respectively. The displacement functions can then be written as:

$$\begin{aligned} u(x,y,z) &= u_0(x,y) + z\phi_x(x,y) \\ v(x,y,z) &= v_0(x,y) + z\phi_y(x,y) \\ w(x,y,z) &= w_0(x,y) \end{aligned} \tag{6}$$

In the case for the von Karman theory, the strain-displacement relation for the in-plane strains are written as:

$$\begin{aligned} \mathbf{e} &= \varepsilon + z\kappa = \varepsilon_m + \varepsilon_\theta + z\kappa \\ \boldsymbol{\gamma} &= \begin{bmatrix} \gamma_{xy} & \gamma_{xz} \end{bmatrix}^T \end{aligned} \tag{7}$$

which, can then be rewritten to be expressed as:

$$
\begin{aligned}
\varepsilon_m &= \begin{bmatrix} u_{,x} & v_{,y} & u_{,y} + v_{,x} \end{bmatrix}^T \\
\varepsilon_\theta &= \frac{1}{2}\begin{bmatrix} w_{,x}{}^2 & w_{,y}{}^2 & 2w_{,x}w_{,y} \end{bmatrix}^T \\
\kappa &= \begin{bmatrix} \phi_{x,x} & \phi_{y,y} & \phi_{x,y} + \phi_{y,x} \end{bmatrix}^T \\
\gamma &= \begin{bmatrix} w_{,y} + \phi_y & w_{,x} + \phi_x \end{bmatrix}^T
\end{aligned} \tag{8}
$$

Furthermore, for the entire model, the displacement *D*, due to the piezoelectric coupling of the elastic and electric fields can be written as in Ref. [5]

$$
\begin{Bmatrix} D_{11} \\ D_{22} \\ D_{33} \end{Bmatrix}_k = \begin{bmatrix} 0 & 0 & 0 \\ 0 & 0 & 0 \\ \bar{e}_{31} & \bar{e}_{32} & 0 \end{bmatrix}_k \begin{Bmatrix} \varepsilon_{11} \\ \varepsilon_{22} \\ \varepsilon_{66} \end{Bmatrix}_k + \begin{bmatrix} \bar{\bar{\Xi}}_{11} & 0 & 0 \\ 0 & \bar{\bar{\Xi}}_{22} & 0 \\ 0 & 0 & \bar{\bar{\Xi}}_{33} \end{bmatrix}_k \begin{Bmatrix} E_{11} \\ E_{22} \\ E_{33} \end{Bmatrix}_k \tag{9}
$$

While, the stress field [σ] is:

$$
\begin{Bmatrix} \sigma_{11} \\ \sigma_{22} \\ \sigma_{33} \end{Bmatrix}_k = \begin{bmatrix} \bar{Q}_{11} & \bar{Q}_{12} & 0 \\ \bar{Q}_{12} & \bar{Q}_{22} & 0 \\ 0 & 0 & \bar{Q}_{66} \end{bmatrix}_k \begin{Bmatrix} \varepsilon_{11} \\ \varepsilon_{22} \\ \varepsilon_{66} \end{Bmatrix}_k + \begin{bmatrix} 0 & 0 & \bar{e}_{31} \\ 0 & 0 & \bar{e}_{32} \\ 0 & 0 & 0 \end{bmatrix}_k \begin{Bmatrix} E_{11} \\ E_{22} \\ E_{33} \end{Bmatrix}_k \tag{10}
$$

Equations (7) and (8) are called the ‘direct’ and ‘converse’ piezoelectric equations. Also, $\bar{e}_{ij}, \bar{Q}_{ij}, \bar{\bar{\Xi}}_{ij}$ are the piezoelectric constants, the plane-stress reduced elastic constants, and the permittivity coefficients, respectively. However, it is often the case wherein the piezoelectric constant matrix [$\bar{e}$] is not readily available for reference [20]. Thus, it is much more convenient to express the piezoelectric constants as the easily available piezoelectric strain constant matrix [*d*] as follows:

$$
\begin{bmatrix} \bar{e} \end{bmatrix} = [d]\begin{bmatrix} \bar{Q} \end{bmatrix} \tag{11}
$$

With these substitutions, the laminate piezoelectric relations can be transformed as in Ref. [5]

$$\begin{Bmatrix} D_x \\ D_y \\ D_z \end{Bmatrix}_k = \begin{bmatrix} 0 & 0 & 0 \\ 0 & 0 & 0 \\ \bar{e}_{31} & \bar{e}_{32} & \bar{e}_{36} \end{bmatrix}_k \begin{Bmatrix} \varepsilon_x \\ \varepsilon_y \\ \gamma_{xy} \end{Bmatrix}_k + \begin{bmatrix} \bar{\bar{\Xi}}_{11} & \bar{\bar{\Xi}}_{12} & 0 \\ \bar{\bar{\Xi}}_{12} & \bar{\bar{\Xi}}_{22} & 0 \\ 0 & 0 & \bar{\bar{\Xi}}_{33} \end{bmatrix}_k \begin{Bmatrix} E_x \\ E_y \\ E_z \end{Bmatrix}_k \tag{12}$$

$$\begin{Bmatrix} \sigma_x \\ \sigma_y \\ \sigma_{xy} \end{Bmatrix}_k = \begin{bmatrix} \bar{Q}_{11} & \bar{Q}_{12} & \bar{Q}_{16} \\ \bar{Q}_{12} & \bar{Q}_{22} & \bar{Q}_{26} \\ \bar{Q}_{16} & \bar{Q}_{26} & \bar{Q}_{66} \end{bmatrix}_k \begin{Bmatrix} \varepsilon_x \\ \varepsilon_y \\ \gamma_{xy} \end{Bmatrix}_k - \begin{bmatrix} 0 & 0 & \bar{e}_{31} \\ 0 & 0 & \bar{e}_{32} \\ 0 & 0 & \bar{e}_{36} \end{bmatrix}_k \begin{Bmatrix} E_x \\ E_y \\ E_z \end{Bmatrix}_k \tag{13}$$

Next, in order to analyze the laminate plate, the force, moment and shear resultant vectors are presented as $\boldsymbol{N_b}$, $\boldsymbol{M_b}$, and $\mathbf{Q}$, respectively. In turn, they can be expressed as:

$$\begin{Bmatrix} \boldsymbol{N_b} \\ \boldsymbol{M_b} \end{Bmatrix} = \begin{bmatrix} \mathbf{A} & \mathbf{B} \\ \mathbf{B} & \mathbf{D} \end{bmatrix} \begin{Bmatrix} \varepsilon \\ \kappa \end{Bmatrix} - \begin{Bmatrix} \boldsymbol{N}_{\Delta T} \\ \boldsymbol{M}_{\Delta T} \end{Bmatrix}$$
$$\mathbf{Q} = [\mathrm{S}]\boldsymbol{\gamma} \tag{14}$$

where ε, κ, $\boldsymbol{N}_{\Delta T}$, $\boldsymbol{M}_{\Delta T}$ and γ are the strain, curvature strain, thermal force, thermal moment, and shear strain, respectively. Additionally, the A, B, D, and S matrices are defined as:

$$\begin{aligned} [\mathbf{A}] &= \sum_{k=1}^{n} \left[\bar{Q}_{ij}\right]_k (z_k - z_{k-1}) \\ [\mathbf{B}] &= \frac{1}{2} \sum_{k=1}^{n} \left[\bar{Q}_{ij}\right]_k (z_k^{\,2} - z_{k-1}^{\,2}) \\ [\mathbf{D}] &= \frac{1}{3} \sum_{k=1}^{n} \left[\bar{Q}_{ij}\right]_k (z_k^{\,3} - z_{k-1}^{\,3}) \\ [\mathbf{S}] &= K \sum_{k=1}^{n} \left[\bar{Q}_{ij}\right]_k (z_k - z_{k-1}) \end{aligned} \tag{15}$$

In this work, the value of *K* is calculated based on Ref. [23]. While the conventional SCF value is acceptable for the analyses of generally thin materials, a better value is necessary for the accurate formulation of thick plates. As such, the SCF, *K*, is calculated as shown in Ref. [23]

$$K_{i3} = \frac{D_{ii}^{\ 2}}{d\int_{-h/2}^{+h/2} \frac{g^2(z)}{G_{13}(z)} dz} \tag{16}$$

where $g(z) = -\int_{-h/2}^{z} \bar{Q}_{11}(z) z_N dz$ and $d = \int_{-h/2}^{+h/2} G_{13}(z) dz$. Additionally, D_{ii} is the bending stiffness in one of the principal direction for K_{13} and K_{23} which are the SCF obtained along *x* and *y* direction, respectively.

The thermal force matrices $\boldsymbol{N_{\Delta T}}$ and $\boldsymbol{M_{\Delta T}}$ are defined as:

$$\begin{aligned} \left[\boldsymbol{N}_{\boldsymbol{\Delta T}}\right] &= \sum_{k=1}^{n} \int_{z_{k-1}}^{z_k} \left[\bar{Q}_{ij}\right]_k \boldsymbol{\alpha_k} \left(z_k - z_{k-1}\right) \boldsymbol{\Delta T} dz \\ \left[\boldsymbol{M}_{\boldsymbol{\Delta T}}\right] &= \sum_{k=1}^{n} \int_{z_{k-1}}^{z_k} \left[\bar{Q}_{ij}\right]_k \boldsymbol{\alpha_k} \left(z_k^{\ 2} - z_{k-1}^{\ 2}\right) \boldsymbol{\Delta T} dz \end{aligned} \tag{17}$$

and the coefficients of thermal expansion matrix, $\boldsymbol{\alpha}$ is expressed as:

$$\boldsymbol{\alpha} = \begin{bmatrix} \alpha_x \\ \alpha_y \\ \alpha_{xy} \end{bmatrix} = \begin{bmatrix} \alpha_1 \cos^2\theta + \alpha_2 \sin^2\theta \\ \alpha_1 \sin^2\theta + \alpha_2 \cos^2\theta \\ 2\left(\alpha_1 - \alpha_2\right) \sin\theta \cos\theta \end{bmatrix} \tag{18}$$

with α_1 and α_2 being the coefficients of thermal expansions in the principal directions and θ the ply-angle of the composite laminate.

2.3 Governing Equations of Motion

The governing equation for this study is derived using the principal of virtual work. Thus, according to the principle of virtual work:

$$\delta \boldsymbol{W} = \delta \boldsymbol{W}_{\text{int}} - \delta \boldsymbol{W}_{\text{ext}} = 0 \tag{19}$$

The internal virtual work δW_{int} can be shown as:

$$\delta \boldsymbol{W}_{\text{int}} = \delta \boldsymbol{d}^{\boldsymbol{T}} \left[\boldsymbol{K} - \boldsymbol{K}_{\Delta \boldsymbol{T}} + \frac{1}{2}\boldsymbol{KN}_1 + \frac{1}{3}\boldsymbol{KN}_2 \right] \boldsymbol{d} - \delta \boldsymbol{d}^{\boldsymbol{T}} \left(\boldsymbol{F} + \boldsymbol{F}_{\Delta \boldsymbol{T}} + \boldsymbol{F}_{\boldsymbol{pie}} \right) \tag{20}$$

where *d* is the displacement vector and $K, K_{\Delta T}, KN_1, KN_2, F, F_{\Delta T}, \text{and } F_{pie}$ represent the linear elastic, thermal geometric, the first-order nonlinear, the second-order nonlinear stiffnesses and the applied, the thermal, and the piezoelectric load vectors, respectively.

The external virtual work δW_{ext} is presented as:

$$\delta \boldsymbol{W}_{\text{ext}} = \delta \boldsymbol{d}^{\boldsymbol{T}} \boldsymbol{M} \ddot{\boldsymbol{d}} - \delta \boldsymbol{d}^{\boldsymbol{T}} \boldsymbol{f} \tag{21}$$

with *M* being the mass matrix and *f* is the external force from the aerodynamic pressure caused by supersonic air flow. According to the first-order piston theory, the assumption is made that the Mach number for the supersonic flow is between the values of $\sqrt{2}$ and 5 [24]. Furthermore, the aerodynamic force is expressed as:

$$p_a(x, y, t) = -\frac{\rho_a V_\infty^{\ 2}}{\sqrt{M_\infty^{\ 2} - 1}} \left[\frac{\partial w}{\partial v} + \left(\frac{M_\infty^{\ 2} - 2}{M_\infty^{\ 2} - 1} \right) \frac{1}{V_\infty} \frac{\partial w}{\partial t} \right] \tag{22}$$

where the variables V_∞ , M_∞, and ρ_a are the air flow speed, Mach number and the air density, respectively.

Furthermore, the non-dimensional aerodynamic pressure is written as:

$$\lambda = \frac{\rho_a V_\infty{}^2 a^3}{\beta^3 D_m} \tag{23}$$

and the non-dimensional aerodynamic damping parameter is given as:

$$g_a = \frac{\rho_a V_\infty \left(M_\infty{}^2 - 2 \right)}{\beta^3 \rho_m h \omega_0} \tag{24}$$

In the damping parameter, the convenient reference frequency ω_0 and the aerodynamic pressure parameter β can be defined as follows:

$$\begin{aligned} \omega_0 &= \sqrt{\frac{D_m}{\rho_m h a^4}} \\ \beta &= \sqrt{M_\infty{}^2 - 1} \end{aligned} \tag{25}$$

However, the parameter can be further simplified by approximating the following terms:

$$\left(\frac{M_\infty{}^2 - 2}{M_\infty{}^2 - 1} \right)^2 \left(\frac{\mu}{\sqrt{M_\infty{}^2 - 1}} \right) \approx \frac{\mu}{M_\infty} \tag{26}$$

where μ is the air-mass ratio defined as $\rho_a a / \rho_m h$ [25]. This approximation is applicable for supersonic air flow. In turn, this allows for Eq. (22) to be reduced as [26]:

$$g_a = \sqrt{\frac{\mu}{M_\infty} \lambda} \tag{27}$$

Thus, the aerodynamic pressure force term of Eq. (21) is then rewritten as:

$$\delta \boldsymbol{d}^T \boldsymbol{f} = \int_A p_a \delta w dA = -\delta \boldsymbol{d}^T \left(\lambda \boldsymbol{A}_f \boldsymbol{d} + \frac{g_a}{\omega_0} \boldsymbol{A}_d \dot{\boldsymbol{d}} \right) \tag{28}$$

Next, the electric fields can be represented as a vector, and also assuming the piezoelectric actuator with a thickness, h_A, and the voltage V^e is applied only in the thickness direction, then the electric field vector $\{E\}$ is expressed as in Ref [5]:

$$\{E\} = \begin{bmatrix} 0 & 0 & 1/h_A \end{bmatrix}^T V^e = [B_v] V^e \tag{29}$$

Then, the final dynamic matrix equation for the element can be written as:

$$\boldsymbol{M}\ddot{\boldsymbol{d}} + \frac{g_a}{\omega_0} \boldsymbol{A}_d \dot{\boldsymbol{d}} + \left[\boldsymbol{K} - \boldsymbol{K}_{\Delta T} + \frac{1}{2}\boldsymbol{K}\boldsymbol{N}_1 + \frac{1}{3}\boldsymbol{K}\boldsymbol{N}_2 + \lambda \boldsymbol{A}_f \right] \boldsymbol{d} = \boldsymbol{F} + \boldsymbol{F}_{\Delta T} + \left[\boldsymbol{K}_{\boldsymbol{av}}^{\boldsymbol{e}} \right] \boldsymbol{V}^{\boldsymbol{e}} \tag{30}$$

Then, in order to analyze the post-buckling behavior, the nonlinear equation is assumed to be the sum of a static and dynamic part, such as $\boldsymbol{d} = \boldsymbol{d}_s + \boldsymbol{d}_t$, where the subscripts ***s*** and ***t*** denote the static and dynamic parts. Then, the static nonlinear equations can be derived as follows:

$$\left[\boldsymbol{K} - \boldsymbol{K}_{\Delta T} + \frac{1}{2}\boldsymbol{K}\boldsymbol{N}_1 + \frac{1}{3}\boldsymbol{K}\boldsymbol{N}_2 + \lambda \boldsymbol{A}_f \right] \boldsymbol{d}_s = \boldsymbol{F} + \boldsymbol{F}_{\Delta T} + \boldsymbol{F}_{\boldsymbol{pie}} \tag{31}$$

Using the Newton-Raphson iterative method, the nonlinear aspect of the model can be calculated using the function $\Psi(\Delta d_s)$, which is defined as:

$$\Psi(\Delta \boldsymbol{d}_s) = \left[\boldsymbol{K} - \boldsymbol{K}_{\Delta T} + \frac{1}{2}\boldsymbol{K}\boldsymbol{N}_1 + \frac{1}{3}\boldsymbol{K}\boldsymbol{N}_2 + \lambda \boldsymbol{A}_f \right] \Delta \boldsymbol{d}_s - \left(\boldsymbol{F} + \boldsymbol{F}_{\Delta T} + \boldsymbol{F}_{\boldsymbol{pie}} \right) \tag{32}$$

In order to iterative over the equation, the tangent stiffness, $\boldsymbol{K}_{\tan_i}$ and the load vectors are derived as:

$$\boldsymbol{K}_{\tan_i} = \left[\frac{\boldsymbol{d}\Psi(\Delta \boldsymbol{d}_s)}{\boldsymbol{d}(\Delta \boldsymbol{d}_s)} \right] = (\boldsymbol{K} - \boldsymbol{K}_{\Delta T} + \boldsymbol{KN}_{1,s} + \boldsymbol{KN}_{2,s} + \lambda \boldsymbol{A}_f)_i$$

$$\Psi(\Delta \boldsymbol{d}_s)_i = \left(\boldsymbol{K} - \boldsymbol{K}_{\Delta T} + \frac{1}{2}\boldsymbol{KN}_{1,s} + \frac{1}{3}\boldsymbol{KN}_{2,s} + \lambda \boldsymbol{A}_f \right)_i \Delta \boldsymbol{d}_s - \left(\boldsymbol{F} + \boldsymbol{F}_{\Delta T} + \boldsymbol{F}_{pie} \right) \tag{33}$$

This is then iterated until the incremental displacement converges.

2.4 Active Control

Finally, in order to analyze the effects of active control of the structure, a damping matrix is required. The damping matrix that is used in the transient response is a sum two different sources of damping: Rayleigh damping and active damping. Rayleigh damping, which is the damping that is inherent in the structure itself, can be expressed as in Ref [5]:

$$C^e = c_1 \left[M^e \right] + c_2 \left[K^e \right] \tag{34}$$

where c_1 and c_2 are coefficients that can be determined from experiments [27] and M and K are the mass and stiffness matrices, respectively.

Next, in order to determine the damping with active control, the external electric field is eliminated and one of the piezoelectric layer is set as a sensor. As the charge is only collected in the thickness direction, the electric displacement vector D is only considered in the z-direction as the electric field vector in the thickness direction only. Then:

$$D_z = e_{31}\varepsilon_x + e_{32}\varepsilon_y + e_{36}\varepsilon_{xy} = \left[e_3 \right] \{ \varepsilon \} \tag{35}$$

Also the charge on the sensor surface is a spatial summation of all charges on each node within

the region of the surface area. Thus, the total charge by summing the closed circuit charge in each layer. Then, as in Ref [3]:

$$q(t)=\sum_{i=1}^{N}\frac{1}{2}\left[\int_{S_i(z=z_k)} D_z dS+\int_{S_i(z=z_{k+1})} D_z dS\right] \tag{36}$$

with N denoting the number of layers and S_i representing the surface of the ith layer.

The current on the surface can be expressed as

$$i(t)=\frac{dq(t)}{dt} \tag{37}$$

This current can then be converted in a voltage through the piezoelectric effect. The output voltage is given as

$$V_{out}(t)=G_c i(t)=G_c\frac{dq(t)}{dt} \tag{38}$$

with G_c being the gain of the current amplifier.

However, the sensor generates a voltage through the oscillation of the piezoelectric structure. When this voltage is fed back into a piezoelectric actuator, the voltage can be calculated by the following equation:

$$V^e=G_i V_s=G_i G_c\frac{dq(t)}{dt} \tag{39}$$

where G_i is the gain to provide feedback control. Thus, the actuator voltage can be rewritten as:

$$V^e=\left[G_i G_c\right]\sum_{i=1}^{N}\frac{1}{2}\left[\int_{S_i(z=z_k)}\left[e_3\right]\left[B\right]dS+\int_{S_i(z=z_{k+1})}\left[e_3\right]\left[B\right]dS\right] \tag{40}$$

or simplified as

$$V^e = [G][K_{sv}]\{\dot{u}\} \tag{41}$$

Then, in the feedback control, the active damping matrix can be defined as

$$[C^*] = -[K_{av}][G][K_{sv}] \tag{42}$$

Therefore, the system of equations of motion for the finite element analysis can be redefined as

$$[\boldsymbol{M}]\ddot{\boldsymbol{d}} + \left([\boldsymbol{C}] + [\boldsymbol{C}^*] + \frac{g_a}{\omega_0}\boldsymbol{A_d} \right)\dot{\boldsymbol{d}} + \left[\boldsymbol{K} - \boldsymbol{K}_{\Delta \boldsymbol{T}} + \frac{1}{2}\boldsymbol{K}\boldsymbol{N}_1 + \frac{1}{3}\boldsymbol{K}\boldsymbol{N}_2 + \lambda \boldsymbol{A_f} \right]\boldsymbol{d} = \left(\boldsymbol{F} + \boldsymbol{F}_{\Delta \boldsymbol{T}} + \boldsymbol{F}_{\boldsymbol{pie}} \right) \tag{43}$$

3. Numerical Results and Discussions

The deformation and the vibrational and buckling responses of a multilayered piezoelectric composite plate is analyzed in a thermal environment and supersonic flow. Additionally, the results are then compared in cases using experimentally determined moduli and micromechanically derived moduli. The structure is composed of four layers of unidirectional composite materials surrounded by two piezoelectric layers. A generalized representation of the structure is shown in Fig. 1. The composite layers in the core of the plate is arranged in a symmetrical stacking sequence of $[\theta/\text{-}\ \theta\ /\text{-}\ \theta\ /\ \theta]\ ^\circ$ unless otherwise indicated. The reference temperature for the thermal environment that is included in this study is set at T_{ref} = 300 K. The finite element model used in the analysis is comprised of a 6x6 mesh with each element consisting of nine nodes, each of which have five degrees of freedom. Finally, there are two different boundary conditions that are used in this study: the simply-supported condition (SS) and the clamped condition (CC). When applying the SS boundary condition, the displacements in the y-axis v and z-axis w as well as the rotation about the y-axis ϕ_y is set to 0 when $x = 0, a$. Also, the displacements in the x-axis u and z-axis w as well as the rotation about the x-axis ϕ_x is set to 0 when $y = 0, b$. Alternatively, for the CC boundary condition, all displacements and rotations are set to 0 when $x = 0, a$ and $y = 0, b$.

3.1 Verifications

Prior to the analysis of the micromechanical moduli, the current finite element model is verified through comparison with previous literatures. First, in order to validate the base linear FEA model that is used in this work, the natural frequencies of the structure are compared to the natural

frequencies of a thin cantilevered piezoelectric composite laminate model as in Ref. [5] and Ref. [28]. In that model, the dimensions are given as $a = b = 20$ cm, and $h = 1.2$ mm. Each composite layer and the piezoelectric layer has a thickness of 0.25 mm and 0.1 mm, respectively. Furthermore, the θ for the ply-angles of the composite core is 45°. The composite material is a T300/976 graphite-epoxy composite and the piezoelectric material is a PZT G1195 piezoceramic. The mechanical properties of the materials re given in Table 1. Comparison of the first five natural frequencies from the current model and from Ref. [5] and Ref. [28] are presented in Table 2 and are found to be in good agreement.

Next, in order to verify the nonlinear portion of the FEA model, the static deflection of a plate with the displacement feedback control system is observed. The plate in this model has the same dimensions as the previous validation model. However, the structure has an SS boundary condition and is also subjected to a uniformly applied load of $q = 100$ N/m^2 as in Ref. [29]. Additionally, instead of both piezoelectric layers being actuator layers, one of them is a sensor layer. Thus, with a feedback control gain G_d, the plate employs a feedback control system wherein the sensor layer generates a voltage in response to the uniform load, which in turn causes the actuator layer to generate a damping force. The deformation of plate with varying G_d values is shown in Fig. 2 with the data from Ref. [29] shown in shaped lines and compared with the results from this work in black circled lines. The deflection calculated from this study is comparing with existing data and are in good agreement, once more validating the current model.

Finally, the inclusion of a thermal environment and supersonic flow is validated with comparison of stability boundaries. The structure that is used for this comparison and in Ref. [30] is a square isotropic plate with a length $a = 12$ in. (30.48 cm) and a thickness $h = 0.05$ in. (0.127 cm). The material properties given in Table 3. Fig. 3 show the stability regions for the structure with non-

dimensional temperature (dT / dT_{cr}) and dynamic pressure λ. Region A represents the region for which the plate is statically and dynamically stable. In contrast Region B and Region C is the region wherein the panel is only statically unstable or only dynamically unstable, respectively. Furthermore, it is shown that the results are in good agreement with Ref. [30].

3.2 Shear Correction Factor (SCF)

The overall purpose of this paper is allow for a greater degree of generalization of the standard composite plate model. In order to facilitate this, an improved SCF values is introduced. While the conventional SCF values are acceptable for the analysis of thin plates, this new SCF scheme also for greater accuracy in regards to thicker plates or plates with lower aspect ratios. Thus, in the current work, the SCF is a function that depends on the thickness ratio, h_f/h. This thickness ratio in turn is determined as the ratio of the thickness of the piezoelectric layer to the thickness of the entire plate. This value is best portrayed in Fig. 4 where the SCF values of at selected thickness ratios and a range of ply-angles are calculated. It is worth noting that for all cases, the improved SCF values, are lower than the conventional SCF. Furthermore, as the thickness ratio increases, which indicates that the piezoelectric layers increase in thickness in comparison to the entire plate, the new SCF diverges farther from the conventional SCF. This shows that the new SCF does change in accordance to the geometry of the plate, thus allowing for the accurate representation to a more general range of plate models. Finally, it is important to note that while the values of K_{13} and K_{23} are different and separate values at most ply-angles, in the case of a 45° ply-angle, the values of K_{13} and K_{23} converge.

3.3 Linear vs Nonlinear Analyses

In this work, the FEA model that was employed uses the Newton-Raphson iterative method for analysis. The majority of the data used in this research is of nonlinear nature due to the fact that there is a clear discrepancy in linear and nonlinear results. This discrepancy is especially apparent for relatively large loads values, as shown in Fig. 5. In both the cases of deflection using the experimental and micromechanical moduli, the nonlinear results diverge from the linear results in a curve. This is particularly observable in the SS boundary condition case. As such, in order to better portray the generalization of the micromechanical model, all results and data in this study are calculated using nonlinear methods, unless otherwise indicated.

3.4 Effective Property Comparison

Currently, plate analysis of composite materials is highly dependent on experiments in order to determine the mechanical properties of the relevant materials used. However, this process is inflexible and greatly restricts what types of composite materials can be used in computational research. To avoid this limitation, a micromechanical model is introduced to calculate the effective properties of the composite using the properties of the constituent materials. This means plate analyses can be conducted with varying fiber volume fractions as well as custom fiber and matrix pairings. As such, a much more holistic study on composite materials can be accomplished. However, an important aspect to this new model is the accuracy of the derived effective properties. Thus, to validate the micromechanical model, the deflections of the structure are compared in cases with and without the effective moduli. In Fig. 6, the maximum deflection values for a plate is given at a range of applied voltages and two selected temperature differentials. The selected temperatures

and the voltage range were selected arbitrarily in an effort to best present the data. The plate that was used for calculation had length $a = b = 20$ cm and thickness $h = 1.2$ mm with each composite layer and piezoelectric layer having a thickness of 0.25 mm and 0.1 mm, respectively. It had an SS boundary condition and the material used was a T300/5208 graphite-epoxy composite. The experimentally determined properties for the composite was well as the constituent materials is given in Table 3. As seen from Fig. 6, the deflection using the experimental and effective properties are in good agreement. Furthermore, it is important to note that in all cases, the deflection was higher when using the micromechanical properties. Conversely, the deflection of the same plate under the same conditions are shown in Fig. 7 with a range of temperatures and two selected applied voltages. Once again, the results are in good agreement and the effective properties characteristically result in slightly higher deflections. However, one very important distinction is that in Fig. 6, the difference between the experimental and effective deflection was constant. But in Fig. 7, the discrepancy increases with the temperature differential. This indicates that the micromechanical model is much more sensitive to thermal environments and may be difficult to utilize in cases of large ΔT.

Additionally, the entire centerline deflection of the plate is shown in Fig. 8 at a constant temperature differential of 5 and with four arbitrarily selected voltages. These voltages were chosen to best represent the shape control capabilities of the piezoelectric layers. The plate was given a uniformly applied load of 200 N/m^2 and is under a SS boundary condition. Also, the material of the plate is the same T300/5208 graphite-epoxy as given in Table 3. Once more, it can be seen that the micromechanical model, while not perfect, is still in acceptable ranges of agreement. Similarly, the plate shown in Fig. 9 has the same conditions and materials, but is under a constant applied voltage of 5 V and an arbitrarily chosen ΔT values. While the two different

centerline deflections are in good agreement, the two centerlines do not converge depending on the applied voltage. Thus, from Fig. 8 and Fig. 9, the observation from Fig. 6 and Fig. 7 are corroborated. The micromechanical model is an acceptable estimation for the experimentally determine moduli, but can become increasingly inaccurate with increasing temperature differential. This can be clearly illustrated in Fig. 10. The same plate under 100 N/m^2 uniform load but with no considerations of the thermal environment shows excellent agreement in the cases with and without the effective moduli. Thus, while it serves as an adequate estimation for plate analysis, if there is to be serious considerations for a thermal environment, a better model is necessary for the coefficients of thermal expansion.

This necessity is highlighted when the effective thermal properties are directly compared with the experimental values. Fig. 11 shows the comparison of the longitudinal coefficient of thermal expansion of various composite materials. The mechanical properties of the constituent materials and the composite materials are from Ref. [35]. The experimentally determined moduli for the composites are displayed with the cross markers. As it can be seen, the current Schapery model is in very good agreement with the actual values. However, in Fig. 12, the transverse coefficient of thermal expansion is compared for the same composite materials using several different micromechanical models. As it can be observed, the current Schapery, while it is not completely accurate, is still the best fit for the majority of the composite materials. In contrast, the current micromechanical model for the transverse Young's modulus and the shear moduli are compared to other models in Fig. 13. While the different models shown in Fig. 12 are varied in accuracy and results, the micromechanical models shown in Fig. 13 are in general close proximity with one another. Thus, while more accurate and form fitting micromechanical models requires further research, for any analysis that involve high temperature differentials, such as the analysis of aircraft

wings or antennae, an improved model for the coefficients of thermal expansion is absolutely necessary.

Finally, the micromechanical model is investigated with consideration for supersonic air flow. Fig. 14 shows the stability regions for the plate structure with non-dimensional temperature (dT / dT_{cr}) and dynamic pressure λ. For cases with and without the micromechanical model, most of the stability boundaries are mostly the same. However, in the case with the effective moduli, the boundary between region C and the chaotic region occurs at slightly lower temperatures. This can once more be attributed to the fact that the micromechanical model produces moduli slightly lower than the experimental moduli. Thus, while the analysis of small deflections and deformations for the plate may be skewed by the relatively inaccurate effective thermal properties, analyses of thermal stability boundaries and dynamic pressures are not as sensitive.

3.5 Applications of the Generalized Model

In the previous section, the validity of the micromechanical model as well as its potential weaknesses have been outlined. However, with the current effective properties, a much more in depth analysis of composite structures can be accomplished. One such example would be a parameter study for the efficiency of different composite materials. In Fig. 15, the specific stiffness for various composite materials are plotted as a function of the fiber volume fraction. From Fig. 15(a), for a given fiber volume fraction, the amount of specific stiffness gained from changing the fiber or epoxy material can be clearly observed. This Fig. 15, in tandem with a basic cost analysis of the composite materials, the efficiency of each material change can be determined. Also, with this type of analysis, a manufacturer of composite materials could calculate the optimal fiber

volume fraction to create the most cost-effective material. Similarly, in Fig. 16, the material efficiency, the ratio between the deflection of the plate and the mass of the entire plate, is graphed as a function of fiber volume fraction for various number of layers. From this figure, it can be clearly observed that adding one more layer to a four-layer composite core always results in a significant increase in efficiency. However, adding one or even two more layers to a five-layer configuration has diminishing returns at high fiber volume fractions. Thus, with the addition of the micromechanical model, optimization of composite materials can be approximated for a case by case basis.

In addition to this, the effective properties can be used for more in depth dynamic analyses. To further analyze the plate structure, the time response of the plate with a thermal environment is conducted with the Newmark β method. The model that is used for this analysis is a four layered composite laminate surrounded by two piezoelectric layers. However, unlike the previous models, one of the piezoelectric layers is a sensor while another is an actuator, thus creating a feedback control system. The dimensions and the ply-angles are the same as well as the material properties given in Table 3. The plate is under a SS boundary condition. The first point of comparison is the temperature differential. Fig. 17 shows the time response of the plate with and without a thermal load with a varying feedback control gain G_d. As expected, as the value of G_d increases, the system experiences a larger amount of damping, thus converging much sooner. However, with the addition of a thermal load, the transient response becomes more varied. As the thermal stiffness matrix decreases the overall global stiffness matrix, the structure has a larger initial amplitude. However, this also allows for the damping matrix to exert a larger force, thus making the plate converge at a faster rate. It is also interesting to note that with the presence of a thermal

environment, the individual effects of the increasing feedback control gain G_d is more obscured. Thus, the micromechanical model can also be utilized for such transient responses.

Next, the different time response for isotropic piezoelectric layers and MFC layers are investigated. The micromechanical model has been applied to the structure for the composite core component. However, as the piezoelectric layers are isotropic, their effective properties cannot be evaluated. But by replacing the piezoelectric layers with MFC, they can be treated as composite materials, thus allowing for the application of the micromechanical model. In addition to this extra level of generalization, the MFC layers can provide a much higher level of shape control to the plate. This is because the unidirectional nature of the MFC allows for a much more directional application of force to the overall structure. This improved shape control can be seen in the transient response shown in Fig. 18. The plate dimension is same as the previous plate structure with the exception that the piezoelectric layer is replaced a MFC layer. The material properties for the MFC layer is given in Table 1 as in Ref. [31]. Due to the improved shape control capabilities of the MFC layer, the dynamic response converges at a much faster rate than compared to the isotropic piezoelectric case.

4. Conclusions

With the application of the RVE micromechanical model, the smart multilayered composite plate model can be generalized. This means that the scope of composite plate analysis can be varied with differing fiber volume fractions and constituent materials. The numerical analysis of the plate with and without effective moduli have shown to be in good agreement. Furthermore, with the application of additional forces such as distributed, thermal or dynamic pressure, the differences in the deformation converged further. Also, with the introduction of an improved SCF, plates of varying thickness ratios can be better accommodated. However, the current micromechanical model is only applicable to the composite core layers. As the piezoceramic on the top and bottom layers are essentially isotropic, its effective moduli cannot be estimated. However, by replacing the piezoelectric layer with MFC layers the RVE method can be applied to the actuators. Additionally, it is shown that the use of MFC layers greatly increases the shape control of the plate. Thus, with these additions, the analysis of smart laminate composite plates can be better adapted and can serve a more flexible purpose.

References

[1] Crawley EF, Javier DL. Use of piezoelectric actuators as elements of intelligent structures. AIAA J 1987;25: 1373-85.

[2] Im S, Atluri SN. Effects of a piezo-actuator on a finitely deformed beam subjected to general loading. AIAA J 1989;27: 1801-07.

[3] Lee CK. Theory of laminated piezoelectric plates for the design of distributed sensors/actuators. Part I: Governing equations and reciprocal relationships. J Acoust Society America 1990;87: 1144-58.

[4] Ha, S. K., Keilers, C., and Chang, F.-K., 1992, "Finite Element Analysis of Composite Structures Containing Distributed Piezoceramics Sensors and Actuators," AIAA J., 30(3), pp. 772–780.

[5] Lam KY, Peng XQ, Liu GR. A finite-element model for piezoelectric composite laminates. Smart Mater Struct 1997;6: 583-91.

[6] Detwiler DT, Shen MH, Venkayya VB. Finite element analysis of laminated composite structures containing distributed piezoelectric actuators and sensors. Finite Elements in Analysis and Design. 1995 Jun 1;20(2):87-100.

[7] Huang JH, Wu TL. Analysis of hybrid multilayered piezoelectric plates. Int J Engn Sci 1996;34: 171-81.

[8] Reddy JN. On laminated composite plates with integrated sensors and actuators. Engn Struc 1999;21: 568-93.

[9] Batra RC, Liang XQ, Yang JS. The vibration of a simply supported rectangular elastic plate due to piezoelectric actuators. Int J Solids Struct 1996;33: 1597-1618.

[10] Moita JMS, Soares CMM, Soares CAM. Geometrically non-linear analysis of composite structures with integrated piezoelectric sensors and actuators. Comp Struct 2002;57: 253-61.

[11] Gao JX, Shen YP. Active control of geometrically nonlinear transient vibration of composite plates with piezoelectric actuators. J Sound Vib 2003;264: 911-28.

[12] Fernandes A, Pouget J. Accurate modelling of piezoelectric plates: single-layered plate. Archive of applied Mechanics. 2001 Aug 1;71(8):509-24.

[13] Fernandes A, Pouget J. Analytical and numerical approaches to piezoelectric bimorph. International journal of solids and structures. 2003 Aug 1;40(17):4331-52.

[14] Fernandes A, Pouget J. Analytical and numerical modelling of laminated composites with piezoelectric elements. Journal of intelligent material systems and structures. 2004 Sep;15(9-10):753-61.

[15] Saviz MR. An optimal approach to active damping of nonlinear vibrations in composite plates using piezoelectric patches. Smart Mater Struct 2015;24(11):115024.

[16] Park CW, Im BU, Shin SJ, Yoon BS, Park JW, Yoon KJ. Numerical and Experimental Analyses of a Smart Fin Using Piezoelectric Actuator. Journal of Aircraft. 2018 Jan 30:1-4.

[17] Lee HJ, Saravanos DA. Coupled layerwise analysis of thermopiezoelectric composite beams. AIAA J 1996;34:1231-7.

[18] Heidary F, Reza Eslami M. Dynamic analysis of distributed piezothermoelastic composite plate using first-order shear deformation theory. J Therm Stresses 2004;27:587-605.

[19] Sladek J, Sladek V, Wünsche M, Tan CL. Crack analysis of size-dependent piezoelectric solids under a thermal load. Engn Fract Mech 2017;182:187-201.

[20] Gibson RF. Principles of composite material mechanics. CRC press; 2016.

[21] Karch C. Micromechanical analysis of thermal expansion coefficients. Modeling and Numerical Simulation Mater Sci 2014;4: 104-18.

[22] Bowles DE. Micromechanics analysis of space simulated thermal deformations and stresses in continuous fiber reinforced composites. 1990.

[23] Birman V and Bert CW. On the choice of shear correction factor in sandwich structures. *J Sandwich Struct Mater* 2002; 4.1: 83-95.

[24] Dixon SC. Comparison of panel flutter results from approximate aerodynamic theory with results from exact inviscid theory and experiment. 1966.

[25] Prakash T, Ganapathi M. Supersonic flutter characteristics of functionally graded flat panels including thermal effects. Composite Structures. 2006; 72.1:10-8.

[26] Liao CL, Sun YW. Flutter analysis of stiffened laminated composite plates and shells in supersonic flow. AIAA journal. 1993; 31.10: 1897-905.

[27] Bathe KJ, Saunders H. Finite element procedures in engineering analysis. 1987.

[28] Chandrashekhar M, Ganguli R. Nonlinear vibration analysis of composite laminated and sandwich plates with random material properties. International Journal of Mechanical Sciences. 2010 Jul 1;52(7):874-91.

[29] Phung-Van P, Nguyen LB, Tran LV, Dinh TD, Thai CH, Bordas SP, Abdel-Wahab M, Nguyen-Xuan H. An efficient computational approach for control of nonlinear transient responses of smart piezoelectric composite plates. International Journal of Non-Linear Mechanics. 2015; 76: 190-202.

[30] Xue DY, Mei C. Finite element nonlinear panel flutter with arbitrary temperatures in supersonic flow. AIAA journal. 1993 Jan; 31.1: 154-62.

[31] Park JS, Kim JH. Suppression of aero-thermal large deflections and snap-through behaviors of composite panels using macro fiber composite actuators. Smart materials and structures. 2004; 13.6: 1448.

[32] Wang W, Dai Y, Zhang C, Gao X, Zhao M. Micromechanical Modeling of Fiber-Reinforced Composites with Statistically Equivalent Random Fiber Distribution. Materials 2016;9: 624-38.

[33] Youssef Z, Jacquemin F, Gloaguen D, Guillen R. A multi-scale analysis of composite structures: application to the design of accelerated hygrothermal cycles. Comp struc 2008;8: 302-9.

[34] Oh IK, Han JK, Lee I. Postbuckling and vibration characteristics of piezolaminated composite plate subject to thermo-piezoelectric loads. J Sound Vib 2000;233: 19-40.

[35] Ran Z, Yan Y, Li J, Qi Z, Yang L. Determination of thermal expansion coefficients for unidirectional fiber-reinforced composites. Chinese Journal of Aeronautics. 2014;27: 1180-7.

Table 1 – Natural frequencies of the piezoelectric laminated composite plate.

Natural Frequency	Present (Hz)	Chandrashekhar [28] (Hz)	Lam [5] (Hz)
1	21.7546	21.5431	21.4655
2	64.6628	63.8273	63.3468
3	130.8899	132.0534	130.8108
4	185.1978	185.3710	182.4012
5	222.7076	224.3175	218.2537

Table 2 – Material properties of PZT G1195N piezoceramics, T300/976 graphite-epoxy composites [5, 32] and MFC [31].

	PZT	**T300/976**	**MFC**
Young's moduli (GPa)			
E_{11}	63.0	150	30.336
$E_{22} = E_{33}$	63.0	9	15.857
Poisson's ratio			
$\nu_{12} = \nu_{21}$	0.3	0.3	0.31
ν_{23}	0.3	0.3	0.16
Shear moduli (GPa)			
$G_{12} = G_{13}$	24.2	7.10	6.130
G_{23}	24.2	2.50	5.906
Density (kg m^{-3})	7600	1600	5115.86
Piezoelectric constants (m V^{-1})			
$d_{31} = d_{32}$	254 x 10^{-12}		400

Table 3. –T300/5208 and constituent properties [33] and piezoceramic properties [34].

	CF T300	**N5208**	**T300/5208**	**PZT5-A**
Young's moduli (GPa)				
E_1	230	2.9	138.7	63
E_2	15	2.9	7.75	63
G_{12}, G_{13}	15	1.07	5.68	24.2
G_{23}	7	1.07	2.94	24.2
Poisson's ratio				
v_{12}	0.2	0.35	0.25	0.3
Coefficients of Thermal Expansion				
α_1 (10^{-6}/K)	-0.07	60	-0.06	0.9
α_2 (10^{-6}/K)	12	60	34.77	0.9
Piezoelectric Strain Constants				
d_{31} (10^{-12}m/V)				254
d_{32} (10^{-12}m/V)				254

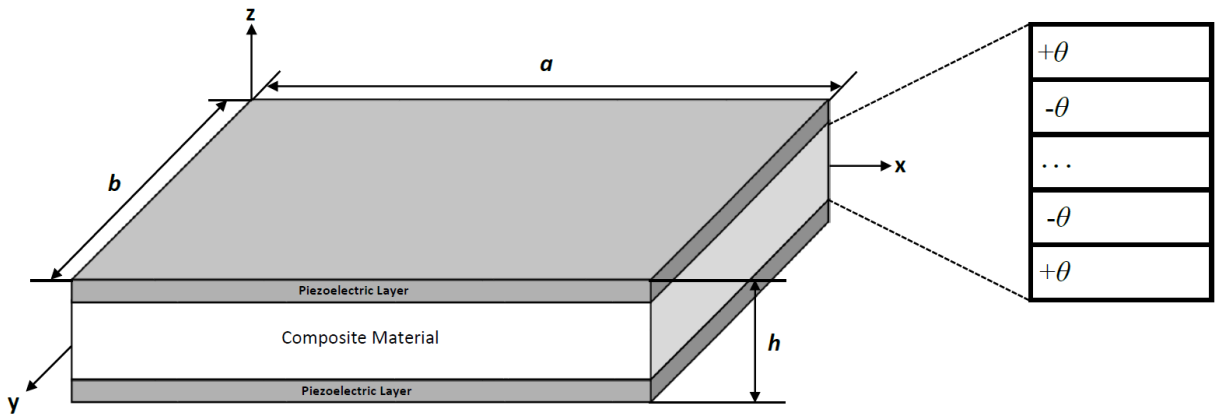

Fig. 1 - Laminated composite plate with piezoelectric layers.

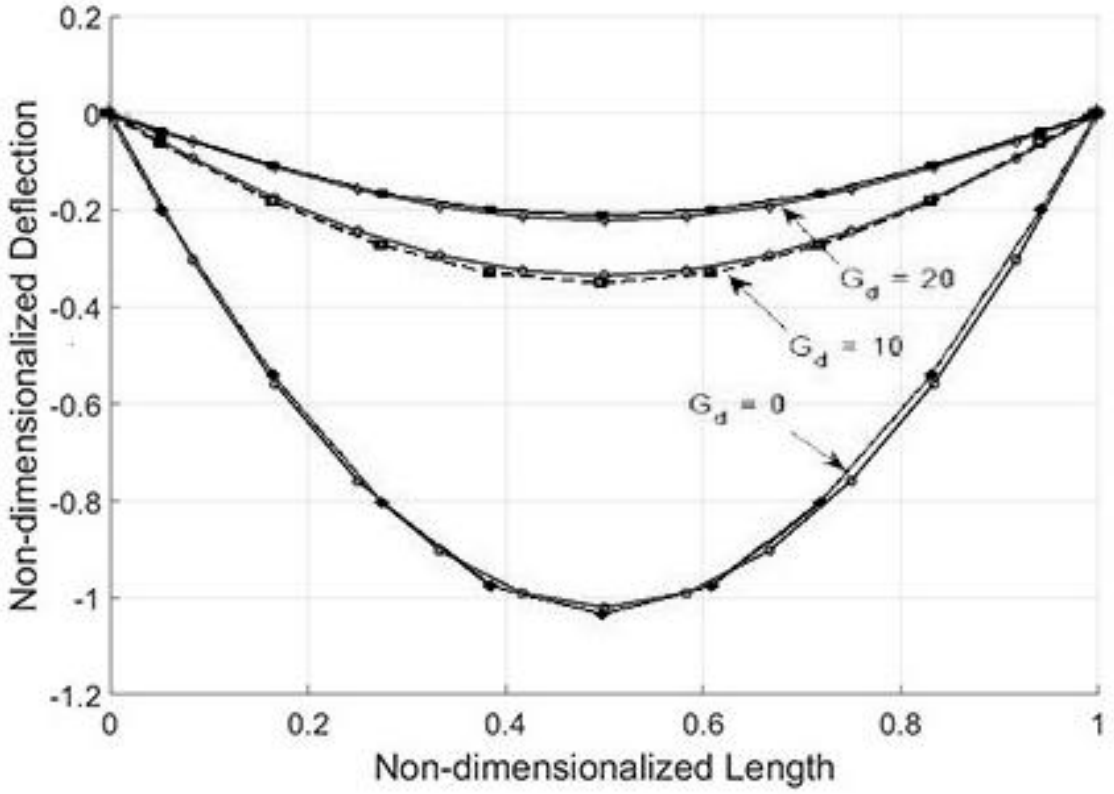

Fig. 2 -Static deflections of the piezoelectric composite plate with differing displacement feedback control gain G_d values.

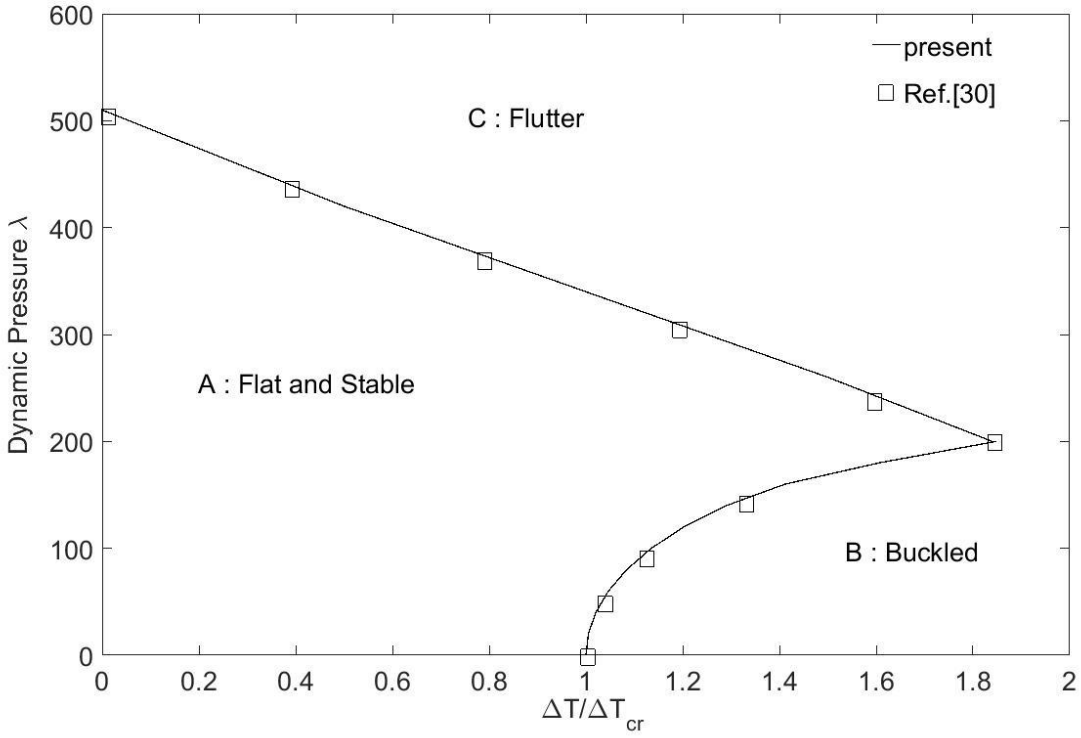

Fig. 3 - Thermal stability boundaries of an isotropic plate.

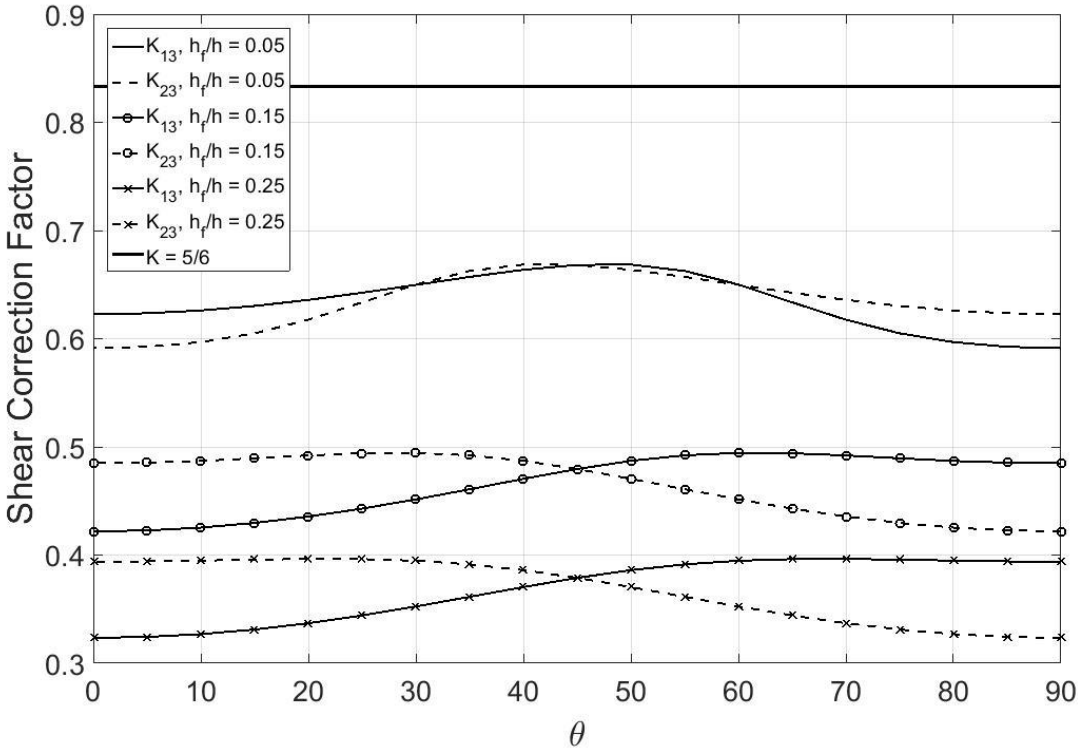

Fig. 4 - SCF at varying ply-angle θ and thickness ratio h_f/h.

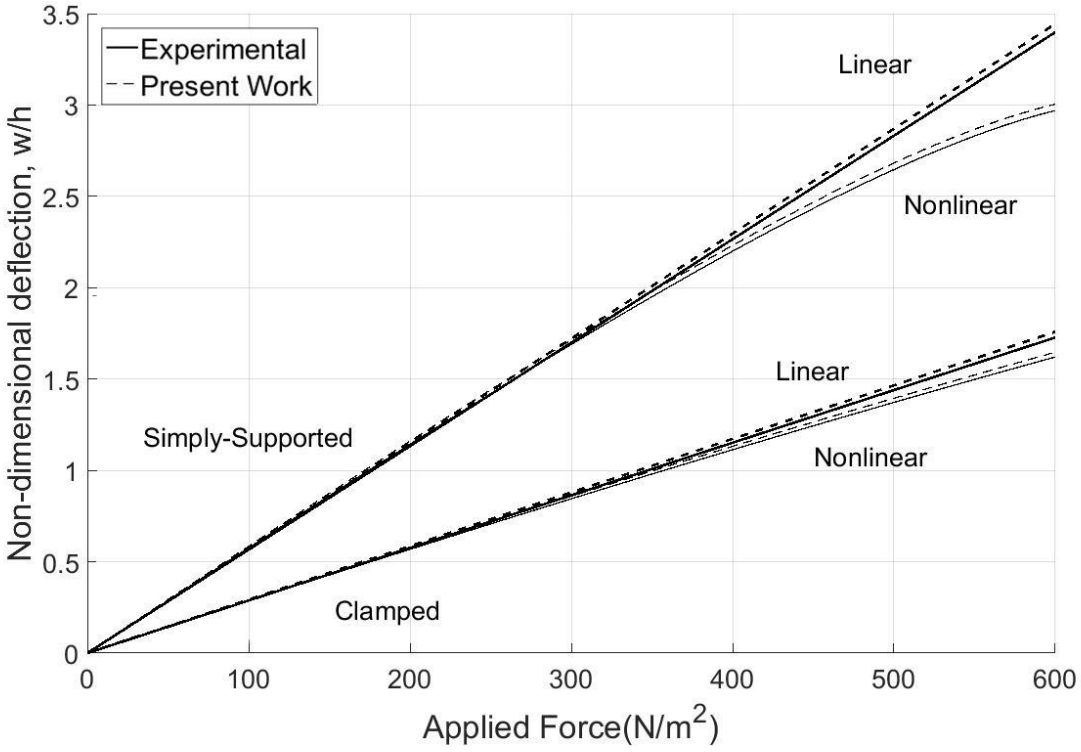

Fig. 5 - Linear and nonlinear deflections of a plate.

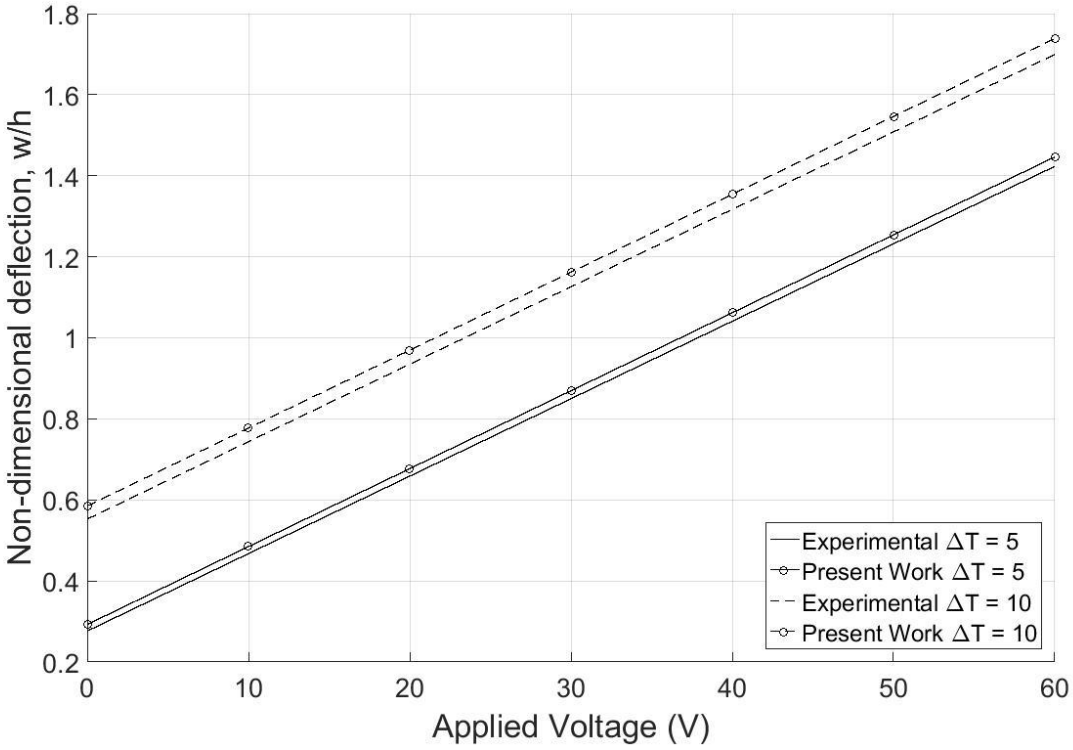

Fig. 6 - Maximum deflections under voltage range and thermal environment.

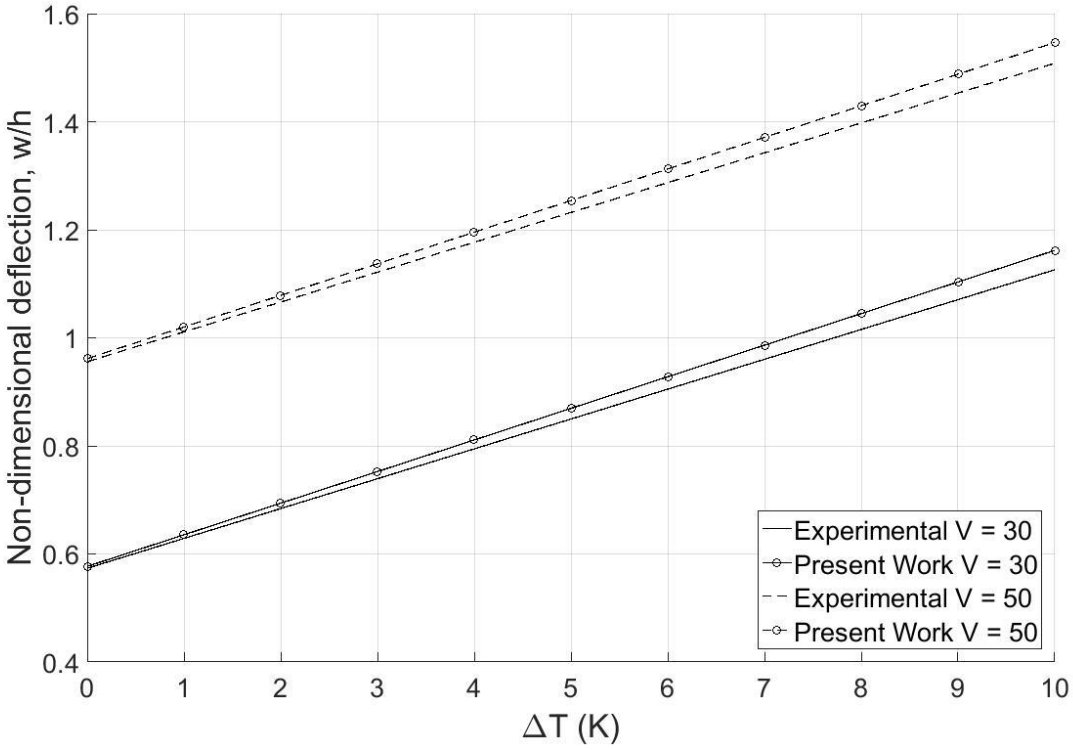

Fig. 7 - Maximum deflections under ΔT range and selected voltages.

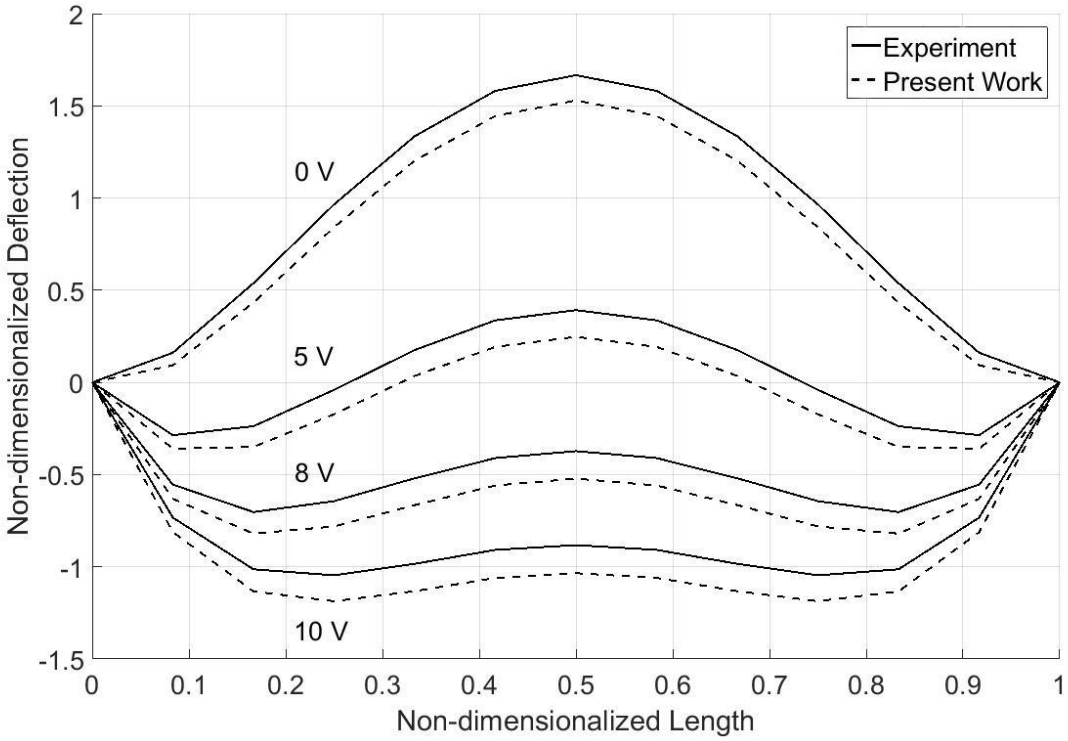

Fig. 8 - Passive shape control with a distributed load and a voltage range in a thermal environment.

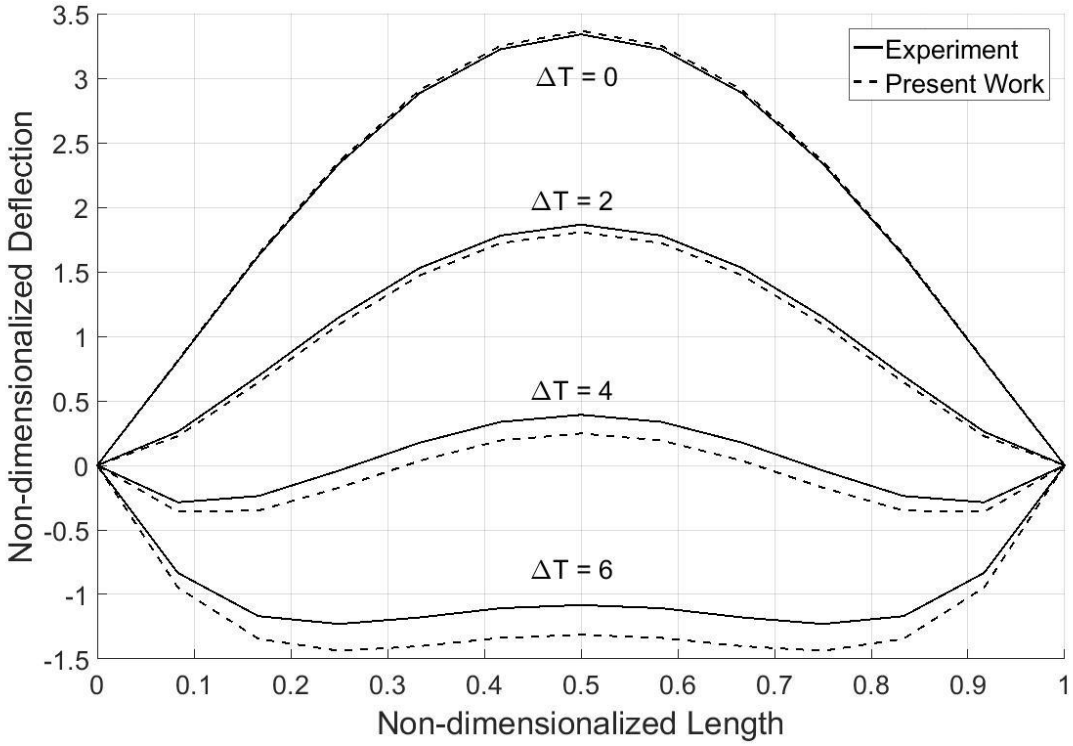

Fig. 9 - Passive shape control with a distributed load and a ΔT range with a selected voltage.

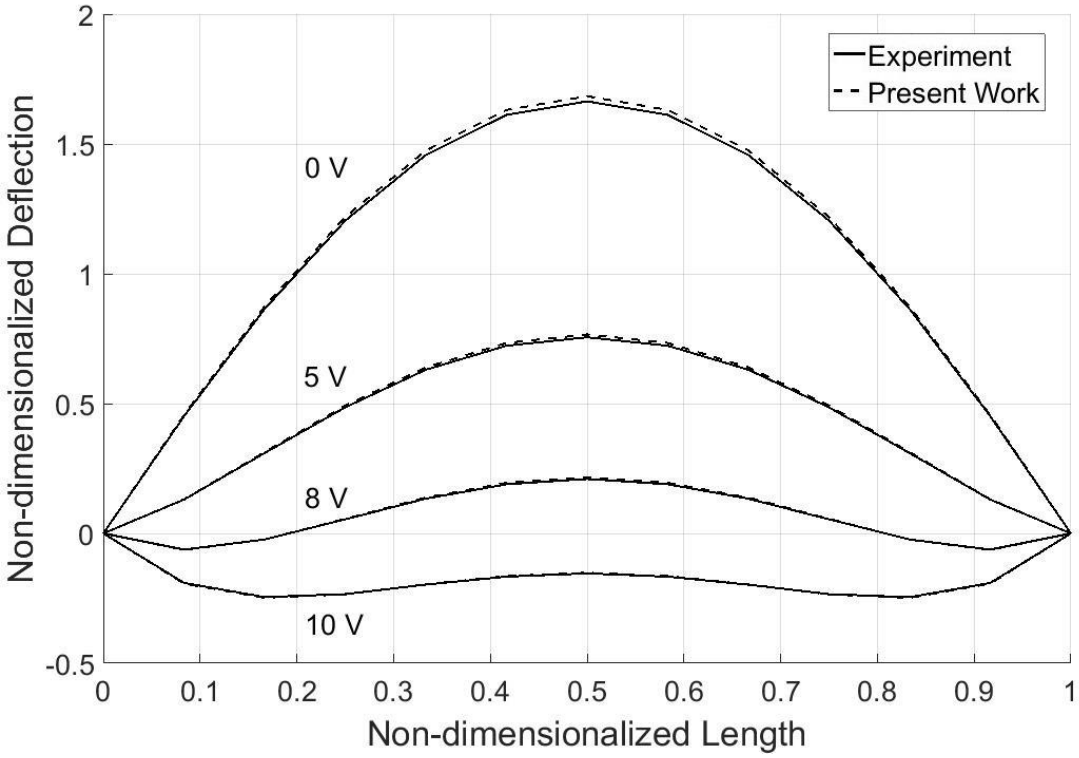

Fig. 10 - Passive shape control with a distributed load and a voltage range.

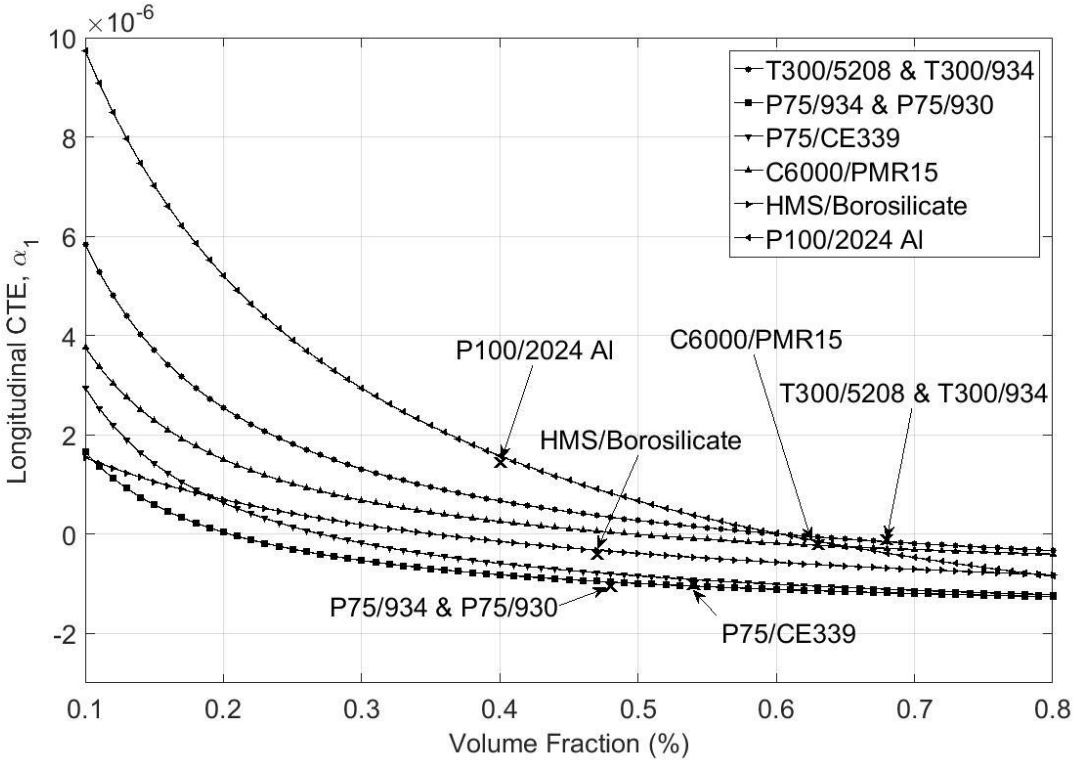

Fig. 11 – Effective longitudinal coefficients of thermal expansion for various composite materials.

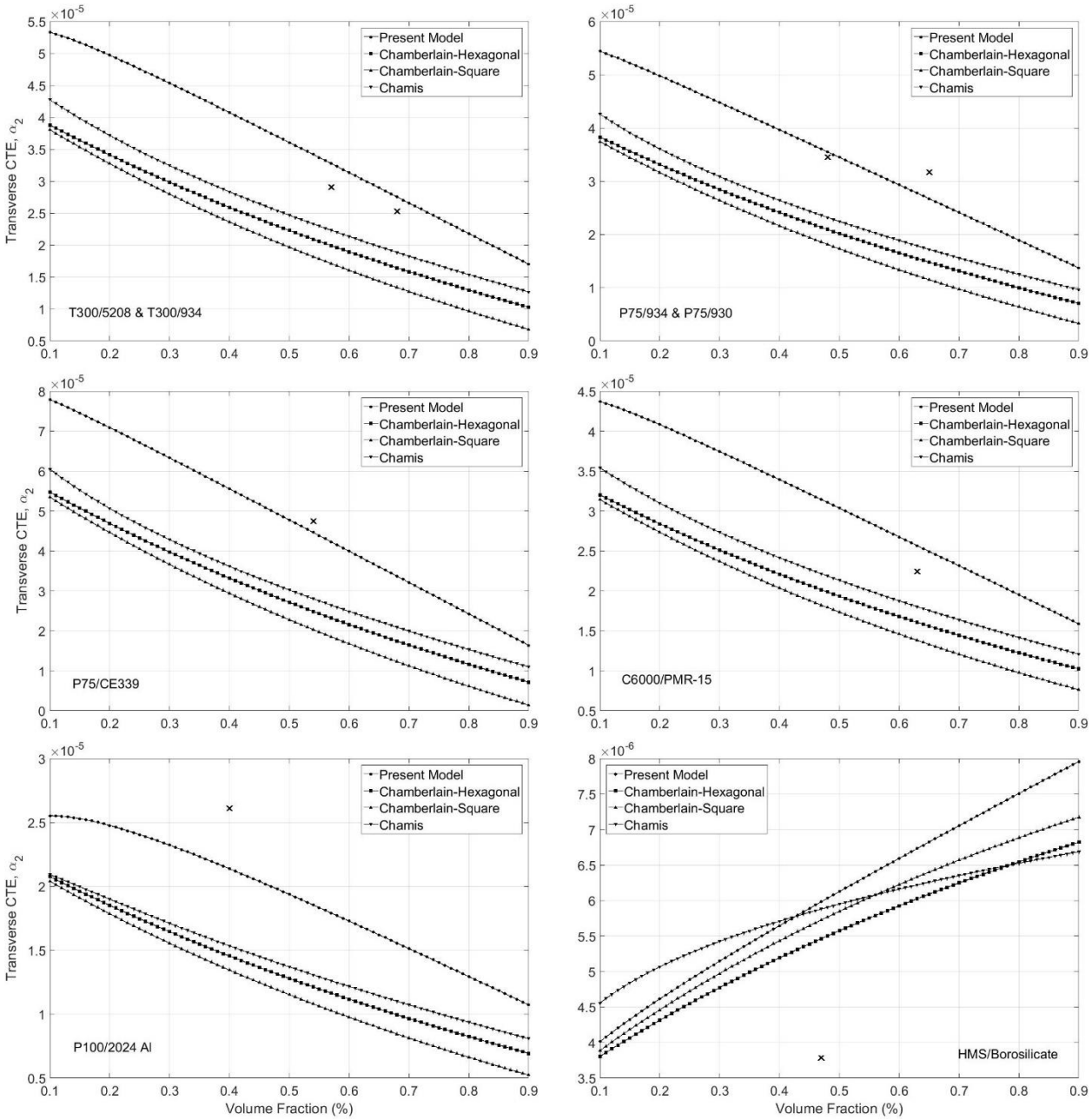

Fig. 12 – Effective transverse coefficients of thermal expansion for various composite materials with different micromechanical models.

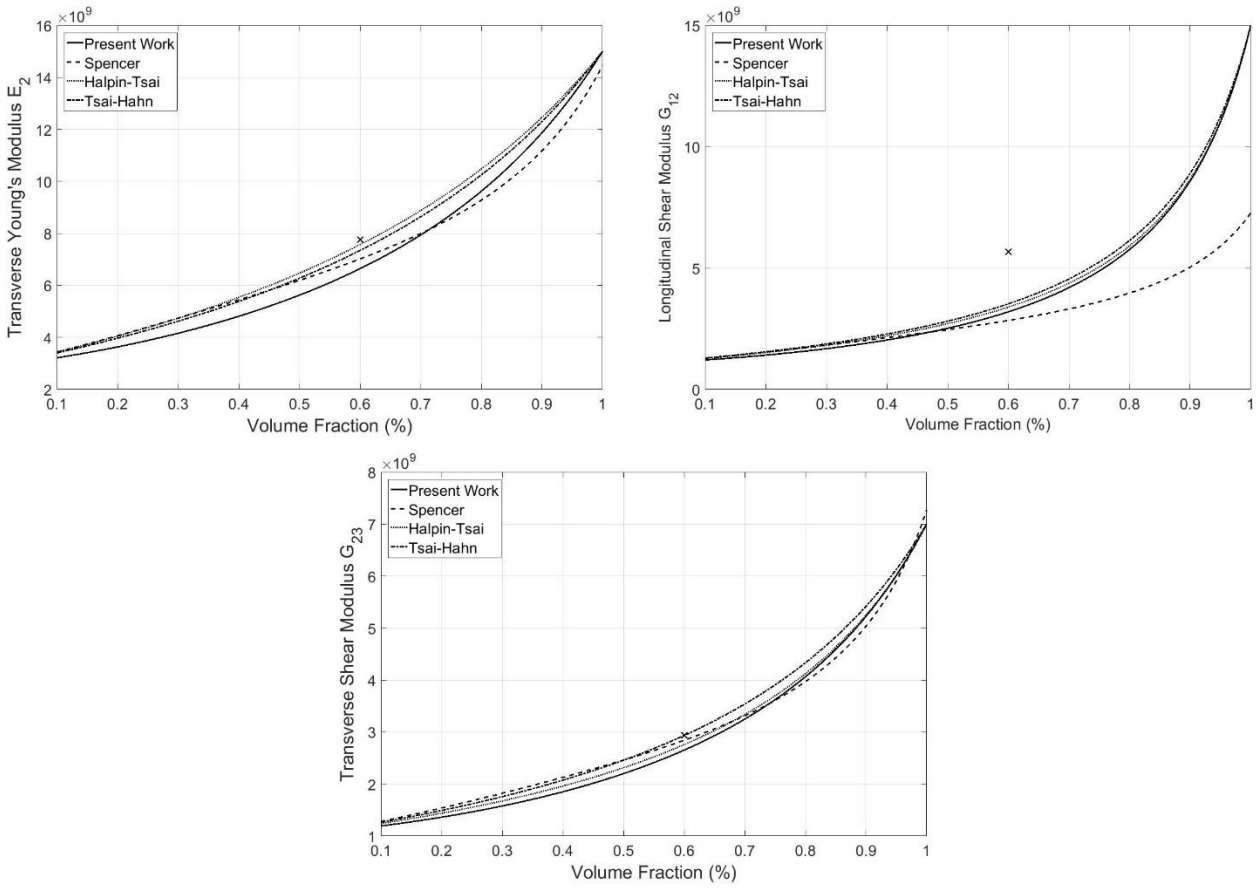

Fig. 13 – Effective moduli with calculated with various different models.

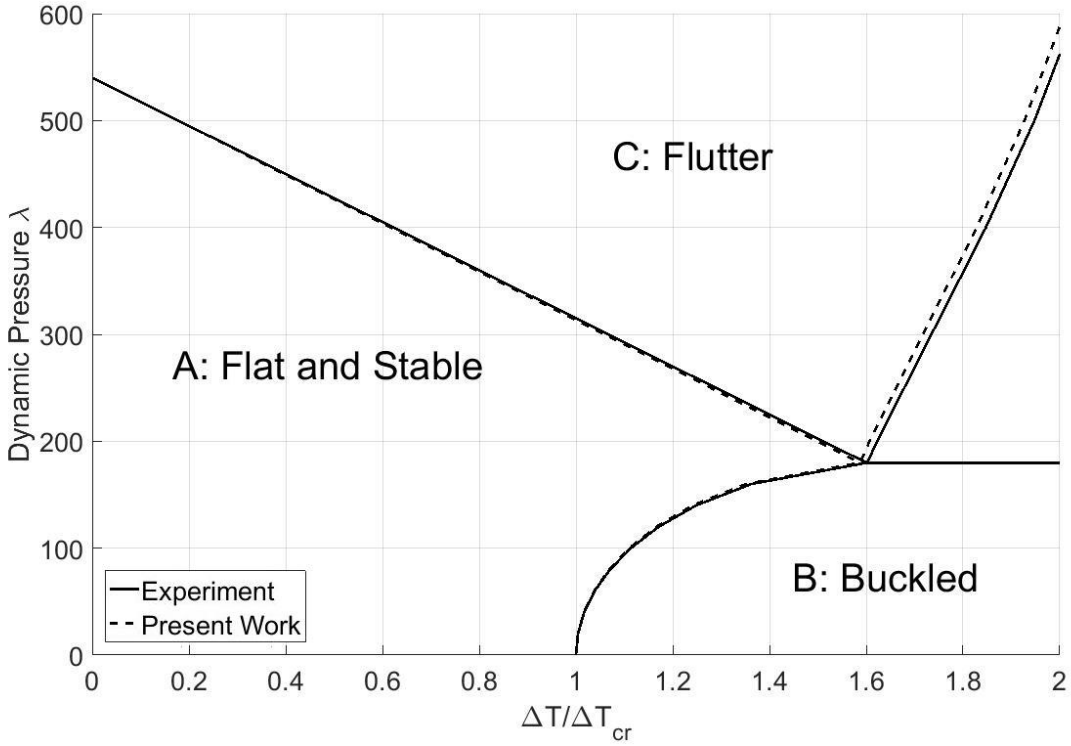

Fig. 14- Thermal stability boundaries of the present model.

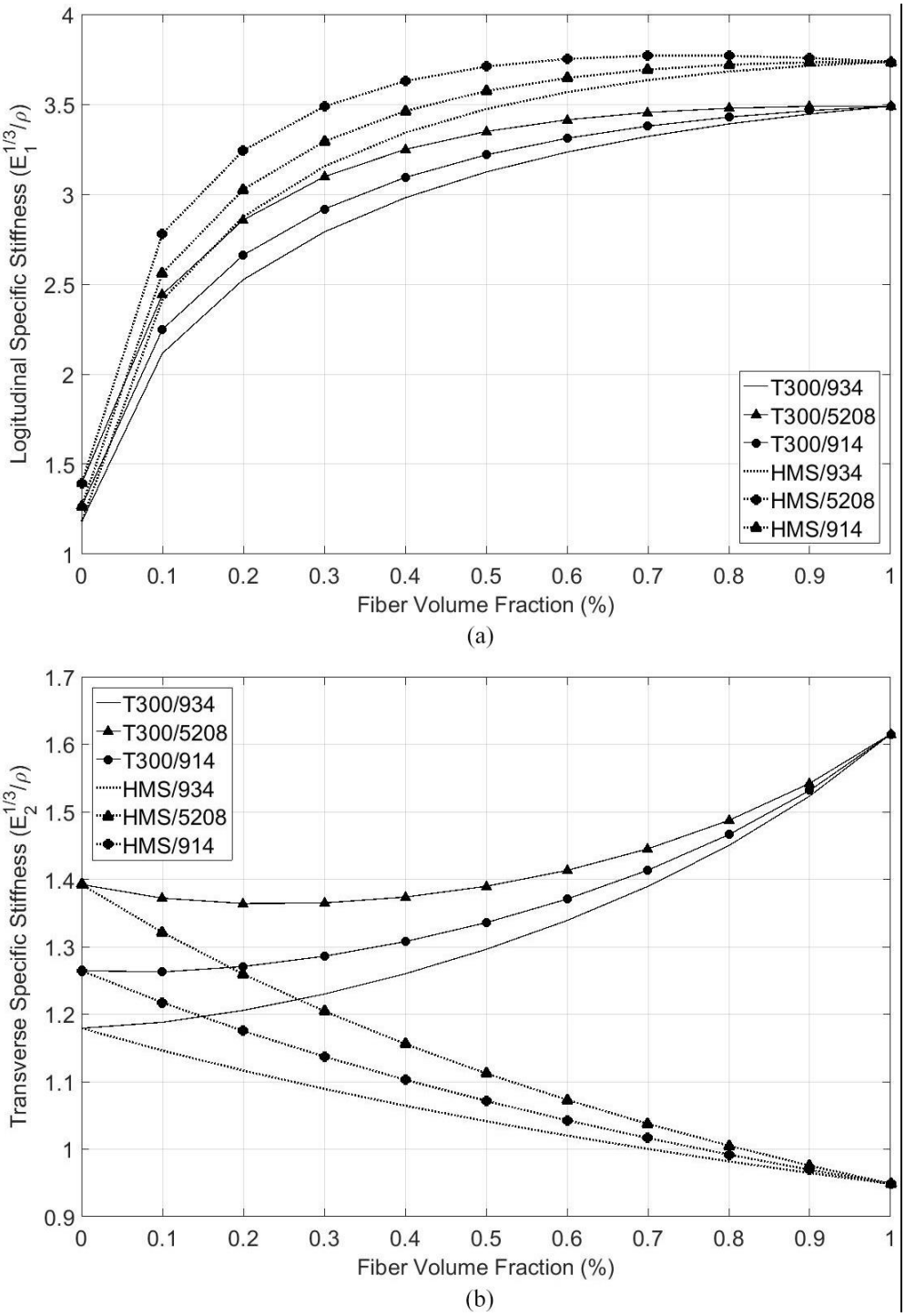

Fig. 15- Specific stiffnesses with varying fiber volume fraction for (a) longitudinal and (b) transverse direction.

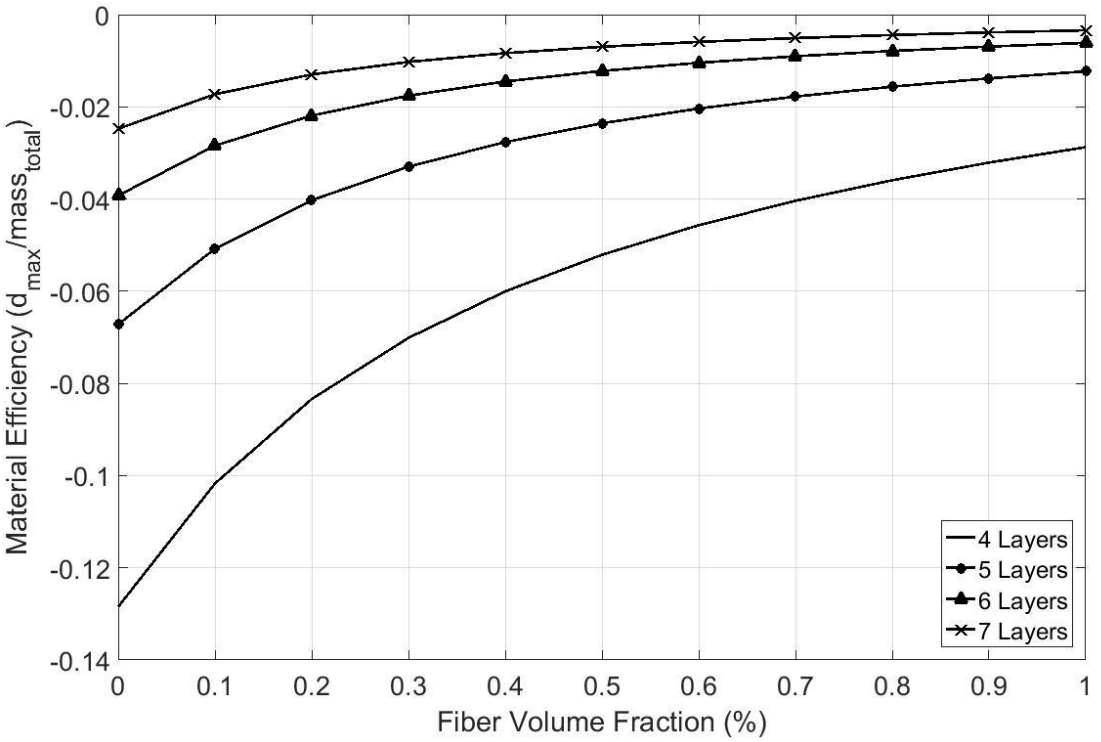

Fig. 16- Material efficiency with varying fiber volume fraction with differing number of layers.

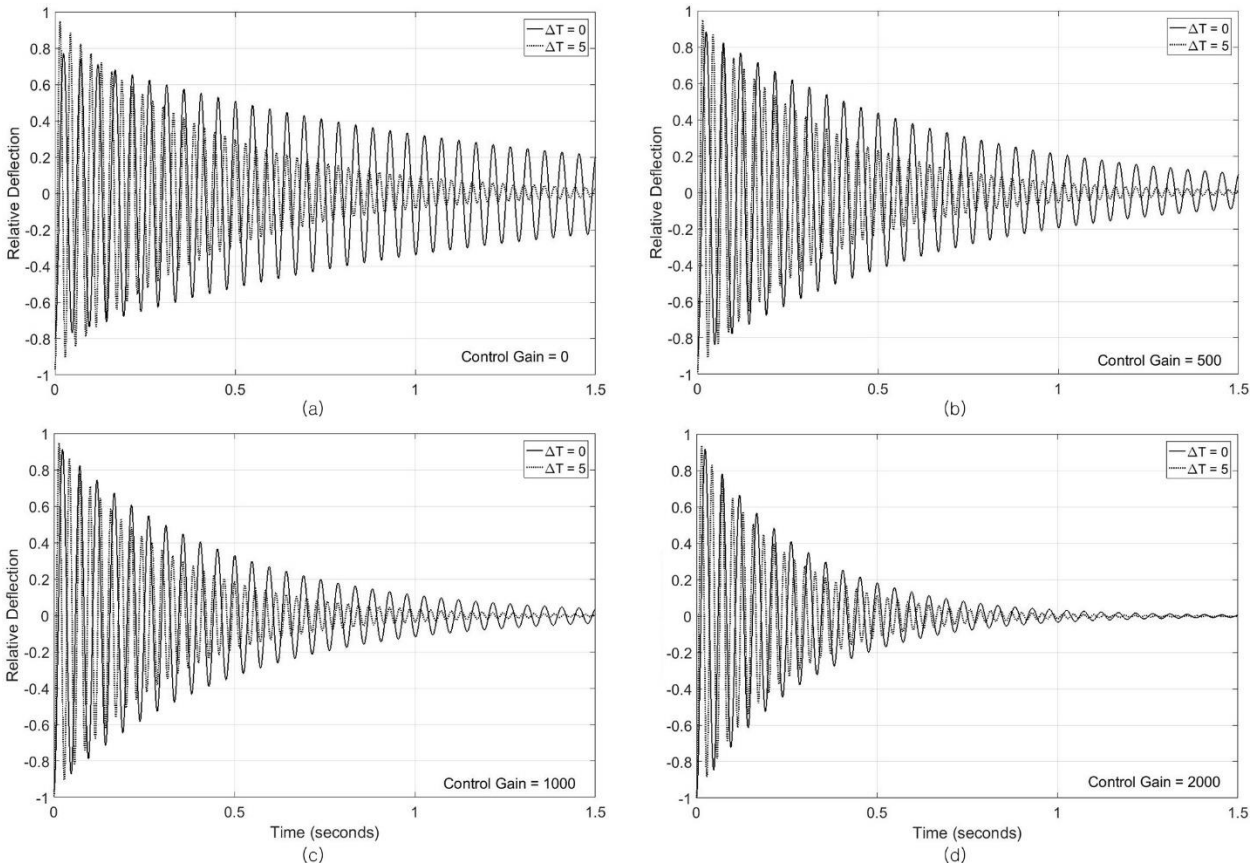

Fig. 17 - Transient response of the plate at various feedback control gain G_d at $\Delta T = 0$ (—) and $\Delta T = 5$ (⋯).

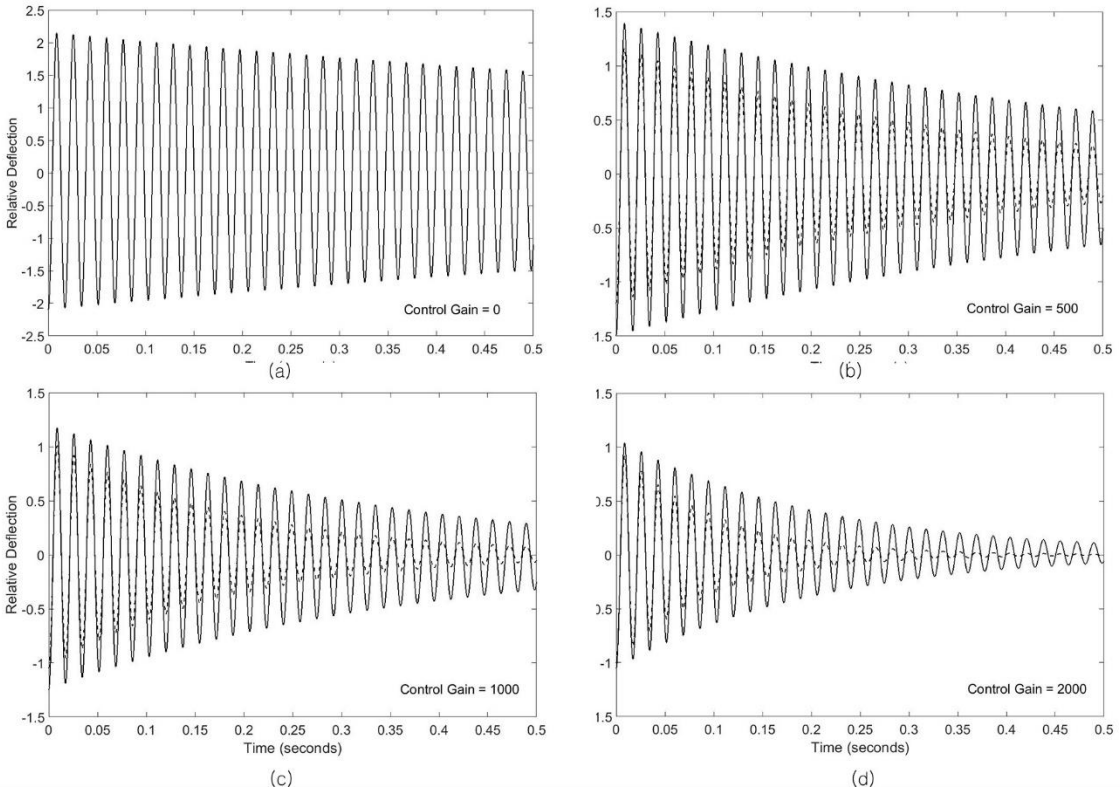

Fig. 18 - Transient response of the plate at various feedback control gain G_d with isotropic (—) and MFC (⋯) piezoelectric layers.

국문 초록

현재 합성 라미네이트의 분석은 실험에 의해 제공되는 재료의 계수에 의해 제한됩니다. 이는 다양한 섬유 부피 분율을 갖는 몇 가지 복합 재료조차도 모듈러스를 결정하는 것이 경제적으로 비현실적이기 때문에 연구를 방해합니다. 솔루션으로 Representative Volume Element (RVE)를 기반으로하는 미소기계적 모델을 적용이 제안됩니다. 이 모델은 유효 계수를 계산하여 복합 재료의 일반화를 허용합니다. 이 연구는 일반 압전 복합 적층판에 적용되는 First-order Shear Deformation Theory of Plates (FSDTP)을 기반으로 한 유한 요소법 (FEM)을 사용합니다. 미소기계적 모듈의 정확성을 검증하기 위해 선형 및 비선형 방법에서 분산 하중, 전압, 온도 및 동적 압력 하에서 구조를 조사합니다. 비선형 해석은 Newton-Raphson Iterative 방법를 사용합니다. 모든 경우에, 마이크로 기계식 모델은 실험 모델과 잘 일치했다. 또한, 개선 된 shear correction factor (SCF)는 두꺼운 판 구조의 맥락에서 더 일반화 있도록 구현됐습니다. 또한, 등방성 압전 층 대신 macro-fiber composite (MFC) 압전 층의 응용이 연구되고있다.

주요어: 미소기계적 모형, 온열 환경, 동압력, 전단 보정 계수, 압전기재료, 비선형 해석, 적층복합재료

학번: 2016-26463